MKPH-T-00-12

The Role of Meson Retardation in Deuteron Photodisintegration above Pion Threshold †

Michael Schwamb and Hartmuth Arenhövel
Institut für Kernphysik, Johannes Gutenberg-Universität, D-55099 Mainz, Germany

Photodisintegration of the deuteron above π threshold is studied in a coupled channel approach including $N\Delta$ and πd channels with consideration of pion retardation in potentials and exchange currents. A much improved description of total and differential cross sections in the energy region between π threshold and 400-450 MeV is achieved. With respect to polarization observables, the description of the linear photon asymmetry and the proton polarization remains problematic.

I. INTRODUCTION

Recently we have constructed in [1], henceforth denoted as I, a realistic hadronic interaction model in the two-nucleon system which takes into account meson retardation completely. This model is based on meson, nucleon and Δ degrees of freedom, and it is able to describe NN scattering quite satisfactorily also above pion threshold. However, for technical reasons it only allows configurations where maximal one meson is present explicitly at a time. Within this restriction, full meson retardation in the potentials has been incorporated in a consistent manner. The motivation for this work was twofold: First of all, from the general principle of relativity any interaction has to be retarded taking into account the finite velocity of its propagation. With respect to the NN interaction, this is particularly evident for energies above pion threshold, where an exchanged pion can become an onshell particle, so that the retarded meson propagator becomes singular describing the coupling of the NN channel to the now open πNN channel. Secondly, there is strong evidence in deuteron photodisintegration above π threshold, in particular in the Δ resonance region, that neglected retardation is one major cause for the failure to describe experimental data by quite sophisticated theoretical treatments which, however, are based on static interactions and corresponding static exchange currents. Indeed, first results have demonstrated clearly the considerable improvement of the theory if retardation is considered [2,3].

In the present work, we have studied deuteron photodisintegration in greater detail with respect to the influences of the various ingredients of the theoretical framework developed in I. In Sect. II we discuss the general structure of the e.m. current operator, which consists of the baryonic components, for example, the one-body spin, convection, and isobar currents, as well as of mechanisms where mesons, especially pions, are created or absorbed. The latter ones are a natural consequence of the incorporation of mesons as explicit degrees of freedom. As is well known, the internal absorption of a photon by a nucleon creating an intermediate Δ isobar is of particular importance in the Δ resonance region. Therefore, Sect. III is devoted to a careful determination of the corresponding $\gamma N\Delta$ coupling by studying the $M_{1+}^{(3/2)}$ multipole in pion photoproduction on the nucleon. In this way, *all* parameters of the theory are fixed in advance before studying electromagnetic reactions in the two-nucleon system. In the following Sect. IV the resulting effective current, acting in the baryonic space only, is derived. Special emphasis is devoted to the structure of the retarded MEC which has, in contrast to its static counterpart, a singular structure above π threshold describing the coupling of the NN to the πNN channel. In Sect. V the question of gauge invariance is discussed. The results for total and differential cross sections as well as for selected polarization observables are presented in Sect. VI. Finally, Sect. VII contains a summary and an outlook.

II. THE ELECTROMAGNETIC CURRENT OPERATOR

The transition amplitude T_{fi}, which describes the absorption of a photon by a hadronic system making a transition from an initial state $|\vec{p}_i, i\rangle$ to a final state $|\vec{p}_f, f\rangle$, is given in Coulomb gauge by the Fourier component of the e.m.

†Supported by the Deutsche Forschungsgemeinschaft (SFB 443).

current matrix element $\vec{J}_{fi}(\vec{k})$

$$\delta^{(3)}(\vec{p}_f - \vec{p}_i - \vec{k})T_{fi} = -\vec{\epsilon}(\vec{k},\lambda)\cdot\vec{J}_{fi}(\vec{k})\,, \tag{1}$$

where the polarization vector of the incoming photon with momentum $\vec{k}$ and helicity λ is denoted by $\vec{\epsilon}(\vec{k},\lambda)$.

A. The general structure of the current

We begin with a brief discussion of the formal structure of the e.m. current. As has been described in detail in I, the model Hilbert space of the two-nucleon system consists of three orthogonal subspaces

$$\mathcal{H}^{[2]} = \mathcal{H}^{[2]}_{\bar{N}} \oplus \mathcal{H}^{[2]}_{\Delta} \oplus \mathcal{H}^{[2]}_{X} \tag{2}$$

containing either two bare nucleons ($\mathcal{H}^{[2]}_{\bar{N}}$), one nucleon and one Δ ($\mathcal{H}^{[2]}_{\Delta}$), or two nucleons and one meson ($\mathcal{H}^{[2]}_{X}$). Accordingly, the current operator can be decomposed into various diagonal and non diagonal components. With the help of the projection operators $P_{\bar{N}}$, P_{Δ}, and P_X onto the above subspaces, respectively (see I), the current $J^\mu(\vec{k})$ can be written as a symbolic 3×3 matrix

$$J^\mu(\vec{k}) = \begin{pmatrix} J^\mu_{\bar{N}\bar{N}}(\vec{k}) & J^\mu_{\bar{N}\Delta}(\vec{k}) & J^\mu_{\bar{N}X}(\vec{k}) \\ J^\mu_{\Delta\bar{N}}(\vec{k}) & J^\mu_{\Delta\Delta}(\vec{k}) & J^\mu_{\Delta X}(\vec{k}) \\ J^\mu_{X\bar{N}}(\vec{k}) & J^\mu_{X\Delta}(\vec{k}) & J^\mu_{XX}(\vec{k}) \end{pmatrix}. \tag{3}$$

Now, we will discuss the various components in detail. We distinguish between pure "baryonic" currents, "one-meson production/annihilation" currents, and the remaining currents, and divide the first one further into one- and two-body operators, labeled by a superscript "[1]" and "[2]", respectively. The diagonal baryonic currents $J^\mu_{\bar{N}\bar{N}}(\vec{k})$ and $J^\mu_{\Delta\Delta}(\vec{k})$ are represented diagrammatically in Fig. 1. The two-body parts comprise effective exchange currents, like for example, heavy meson exchange currents, which are not generated explicitly via the elementary meson-baryon vertices and the meson production/annhilation currents. The transition current $J^\mu_{\Delta\bar{N}}(\vec{k})$, also represented in Fig. 1, describes the e.m. excitation of a Δ resonance including two-body contributions.

The other transition current $J^\mu_{X\bar{N}}$ consists of three components, namely $j^{(0)\,\mu}_{X\bar{N}}$, $j^{(1)\,\mu}_{X\bar{N}}$, and $j^{(1v)\,\mu}_{X\bar{N}}$, where the superscript "(0)" or "(1)" indicates the order with respect to the meson-nucleon coupling constant. Of these, the one-meson production currents $j^{(1)\,\mu}_{X\bar{N}}$ and $j^{(1v)\,\mu}_{X\bar{N}}$ are shown in Fig. 2. Note that the current $J^\mu_{X\Delta}$ is not present because it is set equal to zero (see the discussion in Sect. IV D). In detail, $j^{(1)\,\mu}_{X\bar{N}}$ denotes the contact current which is related to the Kroll-Rudermann term of pion photoproduction, and $j^{(1v)\,\mu}_{X\bar{N}}$ the vertex-current, which is generated by the hadronic vertex form factors. We include in $J^\mu_{X\bar{N}}(\vec{k})$ in general only the pion as most important contribution to the retarded exchange currents with one exception, namely those parts which are necessary for generating the *retarded* $\gamma\pi\rho/\omega$ MEC. This current is of some relevance in deuteron photodisintegration and therefore is taken into account. The remaining current $j^{(0)\,\mu}_{X\bar{N}}$, which is a pure mesonic transition current, is shown in diagram (a) of Fig. 3 together with the two one-body parts of the diagonal component $J^\mu_{XX}(\vec{k})$, describing the coupling of a photon to a nucleon (meson) with a spectating meson-nucleon (nucleon-nucleon) state (see diagrams (b) and (c), respectively). These contributions are denoted as $j^{\bar{N}\,\mu}_{XX}(\vec{k})$ and $j^{X\,\mu}_{XX}(\vec{k})$, respectively. The current $j^{(0)\,\mu}_{X\bar{N}}$ gives an important contribution to the retarded MEC which, however, violates the one-meson-approximation, being another pathology of this approximation which we had alluded to in I. But neglecting it, would lead to a severe violation of gauge invariance for the retarded π MEC. Therefore, it has to be included perturbatively in the construction of the corresponding effective exchange operator.

B. Explicit form of the current components

Most of the currents are obtained by the canonical method of minimal coupling, and the corresponding matrix elements of J^μ are derived in a straightforward manner and need not be given here explicitly. The nucleon one-body current, appearing in $j^{[1]\,\mu}_{\bar{N}\bar{N}}$ and $j^{\bar{N}\,\mu}_{XX}(\vec{k})$, needs some special consideration. Since we start from bare nucleons, the corresponding current $j^{[1]\,\mu}_{\bar{N}\bar{N}}$ is given by a Dirac current with vanishing anomalous magnetic moment κ. However, as discussed in detail in I, the bare nucleon becomes dressed by meson-nucleon loop contributions (see Appendix A of I).

Consequently, the dressed nucleon acquires a nonvanishing anomalous magnetic moment by the presence of this meson cloud (see Fig. 4). However, it is not in agreement with the experimental value as needed for a realistic treatment of photonuclear reactions. Therefore, we substitute the dressed nucleon current of the model by the onshell current with the experimental value for κ. The corresponding nonrelativistic current is denoted by $j^{nr,\,\mu}_{real}(\vec{k})$ and contains the usual convection and spin part. In addition, we also take into account the relativistic spin-orbit current as most important relativistic contribution of leading order. This relativistic contribution is quite important in photodisintegration of the deuteron, even at low energies [4,5].

It is obvious that the above substitution of the physical onshell nucleon current creates formally several inconsistencies. For example, the neglect of the explicit evaluation of the loop diagrams leads to a violation of unitarity if the nucleon current operator is evaluated in the two-nucleon system where the initial and/or final nucleon can become offshell. In this case, some of the loops implicitly present could become singular above pion threshold and, therefore, would lead to an imaginary part describing real meson production.

Now we will consider the remaining current contributions. The matrix elements of the vertex current $j^{(1v)\,\lambda}_{\bar{N}X}$ are given by [6]

$$\langle \bar{N}(\vec{p}\,')|\rho^{(1v)}_{\bar{N}X_\pi}(\vec{k})|\pi(\vec{q},\mu)\bar{N}(\vec{p})\rangle = 0\,, \tag{4}$$

$$\langle \bar{N}(\vec{p}\,')|\vec{j}^{\,(1v)}_{\bar{N}X_\pi}(\vec{k})|\pi(\vec{q},\mu)\bar{N}(\vec{p})\rangle = \delta(\vec{q}+\vec{p}+\vec{k}-\vec{p}\,')\,\frac{g^0_\pi}{2M_N}\,[\hat{e},\tau_\mu]\,(2\vec{q}+\vec{k})\,i\vec{\sigma}\cdot(\vec{q}+\vec{k})\,\frac{F_\pi(\vec{q}^{\,2})-F_\pi((\vec{q}+\vec{k})^{\,2})}{\vec{q}^{\,2}-(\vec{q}+\vec{k})^{\,2}}\,, \tag{5}$$

where $\hat{e}=e\,(1+\tau_3)/2$, and a pion state with momentum $\vec{q}$ and isospin projection μ is denoted by $|\pi(\vec{q},\mu)\rangle$. As next, we identify the nucleon current contribution in the presence of a spectator meson, $j^{\bar{N}\,\mu}_{XX}(\vec{k})$, with the normal nucleon current

$$\langle \pi(\vec{q},\mu)\bar{N}(\vec{p}\,')|j^{\bar{N}\,\lambda}_{XX}(\vec{k})|\pi(\vec{q}\,',\mu')\bar{N}(\vec{p})\rangle = \delta_{\mu\mu'}\;(2\pi)^3\;2\omega(\vec{q})\,\delta(\vec{q}\,'-\vec{q})\,\langle \bar{N}(\vec{p}\,')|j^{nr,\,\lambda}_{real}(\vec{k})|\bar{N}(\vec{p})\rangle\,. \tag{6}$$

The current components for the $\gamma\pi\rho/\omega$ currents cannot be obtained by minimal substitution, but from the usual interaction Lagrangian [7]

$$\mathcal{L}_{\gamma\pi x} = \frac{e g_{\gamma\pi x}}{4m_x}\epsilon_{\mu\nu\lambda\sigma}\,(\partial^\nu A^\mu - \partial^\mu A^\nu)\left(\partial^\sigma \phi^\lambda_x - \partial^\lambda \phi^\sigma_x\right)\phi_\pi \quad \text{with} \quad x\in\{\rho,\omega\}\,. \tag{7}$$

The electromagnetic coupling constants $g_{\gamma\pi x}$, as determined from the decay of the vector meson into a pion and a photon, are [8,9]

$$g_{\gamma\pi\rho}=0.41\,, \quad g_{\gamma\pi\omega}=2.02\,. \tag{8}$$

Now, we will turn to the currents in which a Δ isobar is involved. For the direct electromagnetic exitation $\gamma+\bar{N}\to\Delta$ we take the usual nonrelativistic form which contains a magnetic dipole ($M1$) and an electric quadrupole ($E2$) transition. The analysis of pion photoproduction on the nucleon indicates that the $E2$ transition is largely suppressed compared to the dominant $M1$ transition. Therefore, we neglect the $E2$ contribution and thus take as current [10]

$$\langle \Delta(\vec{p}_\Delta)|\vec{j}_{\Delta\bar{N}}(\vec{k}\,)|\bar{N}(\vec{p}_{\bar{N}})\rangle = e\,\tau_{\Delta\bar{N},\,0}\,\delta(\vec{p}_\Delta-\vec{p}_{\bar{N}}-\vec{k})\,\frac{G^{0\,\Delta\bar{N}}_{M1}}{2M_N}\,i\vec{\sigma}_{\Delta\bar{N}}\times\vec{k}_{\gamma N}\,, \tag{9}$$

with

$$\vec{k}_{\gamma N}=\vec{k}-\frac{M^{res}_\Delta-M_N}{M^{res}_\Delta}\,\vec{p}_\Delta\,, \quad \text{where} \quad M^{res}_\Delta = 1232\,\text{MeV}\,. \tag{10}$$

The corresponding $\gamma\bar{N}\Delta$ charge, which is associated with the current contribution proportional to $\vec{p}_\Delta$, is of minor importance and therefore neglected in this work. The $M1$ strength is determined by fitting the $M^{(3/2)}_{1+}$ multipole amplitude in pion photoproduction on the nucleon which will be the topic of the next section.

At the end of this section we will fix the remaining current contributions $J^\mu_{\Delta\Delta}(\vec{k})$, $J^{[2]\,\mu}_{\bar{N}\bar{N}}(\vec{k})$ and $J^{[2]\,\mu}_{\Delta\bar{N}}(\vec{k})$. Due to the absence of $\Delta\bar{N}$ components in the deuteron wave function, the current $J^\mu_{\Delta\Delta}(\vec{k})$ cannot contribute to the electromagnetic deuteron break-up. $J^{[2]\,\mu}_{\bar{N}\bar{N}}(\vec{k})$ is identified with the ρ MEC $J^{(\rho)\,\mu}(\vec{k})$, which is the most important two-body current besides the π MEC. Note, that first of all in $J^{[2]\,\mu}_{\bar{N}\bar{N}}(\vec{k})$ as well as in $J^{[2]\,\mu}_{\Delta\bar{N}}(\vec{k})$ bare couplings occur, which

have to be renormalized (see Eq. 40 in Sect. IV C). In our approach, $J^{(\rho)\,\mu}(\vec{k})$ is taken in the strictly nonrelativistic form [11]. One should note that, due to the neglect of retardation in $\vec{J}^{\,(\rho)}(\vec{k})$, this MEC is not fully consistent with the ρ exchange of the Elster-Potential which serves as basic NN interaction in this work (see I). Similarly, the second contribution $J^{[2]\,\mu}_{\Delta\bar{N}}(\vec{k})$ is identified with the static pionic Δ MEC $\vec{J}^{\,(\pi)}_{\Delta}(\vec{k})$ in the nonrelativistic limit [12]. In photodisintegration, this current contribution is almost negligible.

III. THE $M^{(3/2)}_{1+}$ MULTIPOLE OF PION PHOTOPRODUCTION

In order to fix the coupling constant $G^{0\,\Delta\bar{N}}_{M1}$ for the $M1$ excitation of the Δ resonance, we now will consider the $M^{(3/2)}_{1+}$ multipole of pion photoproduction on the nucleon. The production amplitude is given by the sum of a Born and a resonance part (see Fig. 5)

$$t_{\pi\gamma}(z) = t^{Born}_{\pi\gamma}(z) + t^{Res}_{\pi\gamma}(z)\,. \tag{11}$$

The resonance part is given in compact form by

$$t^{Res}_{\pi\gamma}(z) = v_{X_\pi\Delta}\, g_\Delta(z)\, \widetilde{j}_{\Delta\bar{N}}(z)\,, \tag{12}$$

where g_Δ denotes the dressed Δ propagator as introduced in I. The effective, energy dependent $\gamma\bar{N}\Delta$ current $\widetilde{j}_{\Delta\bar{N}}(z)$ contains a direct and a rescattering part, i.e.

$$\widetilde{j}_{\Delta\bar{N}}(z) = \frac{j_{\Delta\bar{N}}}{\bar{N}_{[1]}} + v_{\Delta X_\pi}\, g_0(z)\, t^{Born}_{\pi\gamma}(z)\,. \tag{13}$$

where g_0 denotes the nucleon propagator, and $\bar{N}_{[1]}$ a renormalization constant in the one-nucleon sector as defined in the Appendix A of I.

The dominant contributions to the Born amplitude to the $M^{(3/2)}_{1+}$ amplitude are displayed in Fig. 6. They consist of the time ordered pion pole diagrams and the crossed nucleon pole diagram. Following the procedure in [13], less important mechanisms like ω exchange will be taken into account effectively by a parameter b which is close to unity. Thus we use explicitly as Born amplitude

$$\begin{aligned}\langle\pi(\vec{q}\,\mu)N(-\vec{q})|t^{Born}_{M^{(3/2)}_{1+}}(z)|\gamma(\vec{k})\bar{N}(-\vec{k})\rangle = &-b\,\frac{g_\pi}{2M}[\hat{e},\tau^\dagger_\mu]\,\vec{\epsilon}\cdot(2\vec{q}-\vec{k})\,i\vec{\sigma}\cdot(\vec{q}-\vec{k})\,F_\pi((\vec{q}-\vec{k})^{\,2})\\
&\times\frac{1}{2\omega(\vec{q}-\vec{k})}\left[\frac{1}{z-k-\omega(\vec{q}-\vec{k})-e^{nr}_N(\vec{q})}+\frac{1}{z-\omega(\vec{q})-\omega(\vec{q}-\vec{k})-e^{nr}_N(\vec{k})}\right]\\
&-b\,\frac{g_\pi}{4M^2_N}\,\frac{\hat{e}\tau^\dagger_\mu\,\vec{\epsilon}\cdot(2\vec{q}+\vec{k})\,i\vec{\sigma}\cdot\vec{q}+(\hat{e}+\hat{\kappa})\tau^\dagger_\mu\,\vec{\epsilon}\cdot\vec{\sigma}\times\vec{k}\,\vec{\sigma}\cdot\vec{q}}{z-k-\omega(\vec{q})-e^{nr}_N(\vec{q}+\vec{k})}\,F_\pi(\vec{q}^{\,2})\,,\end{aligned} \tag{14}$$

where the form factor F_π and the pion-nucleon coupling constant g_π are given by the underlying NN interaction (here the Elster-potential, see Table I in I). The parameter b and the renormalized $\gamma\bar{N}\Delta$ coupling constant $G^{\Delta\bar{N}}_{M1} = G^{0\,\Delta\bar{N}}_{M1}/\bar{N}_{[1]}$ are fitted to the experimental data of Arndt *et al.* [14] (solution SM97K) yielding

$$G^{\Delta\bar{N}}_{M1} = -3.91 \;\;\text{and}\;\; b = 0.84\,. \tag{15}$$

We would like to emphasize that Watson's theorem [15] is exactly fulfilled below two-pion threshold. In view of small but significant differences of the experimental P_{33}-phases determined from πN scattering versus pion photoproduction, we have determined $G^{\Delta\bar{N}}_{M1}$ and b as well as the hadronic parameters $f^0_{\Delta\pi N}$, $\Lambda_{\Delta\pi N}$, and M^0_Δ by a *simultaneous* fit of the $M^{(3/2)}_{1+}$ multipole and the P_{33} partial wave of πN scattering (see Figs. 7 and 8).

As next, we would like to introduce the effective strength $\widetilde{G}^{\Delta\bar{N}}_{M1}(z,k)$ which is defined by the matrix element of the effective current $\widetilde{j}^{\,\mu}_{\Delta\bar{N}}(z)$ in the Δ rest frame

$$\langle\Delta(\vec{p}_\Delta=0)|\vec{\widetilde{j}}_{\Delta\bar{N}}(z,\vec{k})|\bar{N}(\vec{p}_{\bar{N}})\rangle = e\,\tau_{\Delta\bar{N},\,0}\,\delta(\vec{p}_{\bar{N}}+\vec{k})\,\frac{\widetilde{G}^{\Delta\bar{N}}_{M1}(z,k)}{2M_N}\,i\vec{\sigma}_{\Delta\bar{N}}\times\vec{k}\,, \tag{16}$$

where for initial onshell nucleons z and k are related by $z = W + i\epsilon$ with $W = e^{nr}_N(\vec{k}) + k$. In the later discussion of the results this coupling will be referred to as $\widetilde{G}^{\Delta\bar{N}}_{M1}$(eff1). Because of the occurrence of intermediate pion-nucleon

loops in the rescattering amplitude (see Fig. 5), $\widetilde{G}_{M1}^{\Delta\bar{N}}(z,k)$ becomes complex above π threshold. Modulus $\widetilde{\mu}_{\Delta N}(W,k)$ and phase $\widetilde{\Phi}(W,k)$ of the effective coupling

$$\widetilde{G}_{M1}^{\Delta\bar{N}}(z=W+i\epsilon,k)=\widetilde{\mu}_{\Delta N}(W,k)\,e^{i\widetilde{\Phi}(W,k)} \tag{17}$$

are shown by the full curves in Fig. 9. Obviously, the energy dependence of the modulus is rather weak.

Finally, we would like to compare briefly the effective $\gamma\bar{N}\Delta$ coupling of Wilhelm *et al.* [12,16]. Similar to [17,18], the onshell matrix element of the resonant amplitude together with the Born terms are fitted directly to experimental data without explicitly evaluating the rescattering amplitude. The parameters b and F_π are set equal to one, and the energy dependent ansatz is used

$$\widetilde{\mu}_{\Delta N}(W,k)=\mu_0+\mu_2\left(\frac{q}{m_\pi}\right)^2+\mu_4\left(\frac{q}{m_\pi}\right)^4 \quad\text{and}\quad \widetilde{\Phi}(W,k)=\frac{q^3}{a_1+a_2q^2}\,, \tag{18}$$

where $W=e_N^{nr}(\vec{q})+\omega_\pi(\vec{q})$ and q denotes the momentum of the outgoing pion. The free parameters are fitted to the data of Berends and Donnachie [19]. This coupling, denoted henceforth by $\widetilde{G}_{M1}^{\Delta\bar{N}}$(eff2), is represented by the dotted curves in Fig. 9. Note that the modulus of this coupling is considerably smaller at low energies than the one of our approach, where the rescattering amplitude is explicitly evaluated. As will be seen in Sect. VI, this feature turns out to be one of the reasons for the considerable underestimation of the total cross section of deuteron photodisintegration in [12,16].

IV. THE EFFECTIVE CURRENT OPERATOR IN DEUTERON PHOTODISINTEGRATION

After having fixed all current components of (3), we will now construct an effective current operator, which acts in pure hadronic space, by eliminating all explicit meson d.o.f. It is defined by

$$\langle f|PJ_{eff}^{\mu}(z,\vec{k})P|i\rangle=\langle f|J^{\mu}(\vec{k})|i\rangle\,. \tag{19}$$

The initial and final states are given by the effective deuteron and outgoing NN scattering states, respectively. Their explicit forms are given in (55) and (47) through (49) of I. We will evaluate the effective current in the antilab system, where the final NN scattering state is at rest and the deuteron has total momentum $-\vec{k}$. In principle, one would then need a boost contribution for the moving deuteron which, however, can safely be neglected according to the findings in [20].

Inserting the various components of the current into the rhs of (19), it turns out that the effective current operator can be split into a nucleonic and a resonant part with superscripts "N" and "Δ", respectively, which in turn can be divided into one- and two-body terms denoted by superscripts "[1]" and "[2]", respectively (see Fig. 10)

$$J_{eff}^{\mu}(z,\vec{k})=J_{eff}^{N[1]\,\mu}(z,\vec{k})+J_{eff}^{\Delta[1]\,\mu}(z,\vec{k})+J_{eff}^{N[2]\,\mu}(z,\vec{k})+J_{eff}^{\Delta[2]\,\mu}(z,\vec{k})\,. \tag{20}$$

We would like to remark, that in this evaluation we have included perturbatively the contributions from the one-meson-approximation violating diagram (a) of Fig. 3. In this context, we have to introduce into the corresponding expressions below projection operators $P_{x_1x_2}$ on a state consisting of two nucleons and two mesons of type x_1 and x_2.

A. The nucleonic one-body contribution $J_{eff}^{N[1]\,\mu}(z,\vec{k})$

According to the discussion in subsection II B, this component is represented by the physical onshell current including the relativistic spin-orbit part

$${}^{(-)}\langle NN;\vec{p},\alpha|PJ_{eff}^{N[1]\,\mu}(z,\vec{k})P|d\rangle=\frac{1}{N_d}\,{}^{(-)}\langle NN;\vec{p},\alpha|P_{\bar{N}}\frac{\widehat{Z}_{[2]}^{os}}{\widehat{R}(z)}\sum_{i=1,2}\Big(j_{real}^{nr,\,\mu}(i,\vec{k})+j^{so\,\mu}(i,\vec{k})\Big)P_{\bar{N}}|d\rangle\,, \tag{21}$$

where α characterizes additional quantum numbers, and the normalization constant N_d is given in Eq. (56) of I. It differs from unity in retarded approaches only (e.g., $N_d=0.992$ for the Elster-potential).

B. The resonant one-body contribution $J_{eff}^{\Delta[1]\,\mu}(z,\vec{k})$

The component $J_{eff}^{\Delta[1]\,\mu}(z,\vec{k})$ is given essentially by the effective $\gamma\bar{N}\Delta$ current

$$ {}^{(-)}\langle NN;\,\vec{p},\alpha)|P_\Delta J_{eff}^{\Delta[1]\,\mu}(z,\vec{k})P_{\bar{N}}|d\rangle = \frac{1}{N_d}{}^{(-)}\langle NN;\,\vec{p},\alpha)|P_\Delta \sum_{i,j=1,2;\,i\neq j}\Big(\widetilde{j}^{\,\mu}_{\Delta\bar{N}}(i,z-e_N(\vec{p}_j),\vec{k})\Big)\hat{R}^\pi(z-k)P_{\bar{N}}|d\rangle\,. \quad (22) $$

Note that similar to the Elster-Potential, we consider only pion-nucleon loops in $\hat{R}^\pi(z-k)$. The effective current $\widetilde{j}^{\,\mu}_{\Delta\bar{N}}(z)$ has the same functional form as given in (9) except that $G_{M1}^{0\,\Delta\bar{N}}$ is replaced be the effective excitation strength $\widetilde{G}_{M1}^{\Delta\bar{N}}(W_{sub}+i\epsilon,k_{\gamma N})$, where

$$ W_{sub}(W,\vec{p}_\Delta) = W - M_N - \frac{\vec{p}_\Delta^{\,2}}{2\mu_{N\Delta}} \quad (23) $$

denotes the invariant mass of the πN subsystem which we have evaluated for the spectator onshell choice. In the actual evaluations in the two-nucleon system, $\widetilde{G}_{M1}^{\Delta\bar{N}}$ is calculated in the rest frame of the Δ, similar to the treatment in the $M_{1+}^{(3/2)}$ multipole. The difference with respect to the one-nucleon sector is that $k_{\gamma N}$ and W_{sub} are *not* related by an onshell relation, i.e., $e_N^{nr}(k_{\gamma N})+k_{\gamma N}\neq W_{sub}$. Because of the explicit evaluation of the pion-nucleon loop in the rescattering Born amplitude (cut A in diagram (c) of Fig. 5), this feature does not lead to any complications in practice. On the other hand, in the treatment of Wilhelm *et al.* [16] such an offshell extrapolation of $\widetilde{G}_{M1}^{\Delta\bar{N}}$ is not possible. Therefore, they have used an onshell prescription

$$ \widetilde{G}_{M1}^{\Delta\bar{N}}(W_{sub}+i\epsilon,k_{\gamma N}) \to \begin{cases} G_{M1}^{\Delta N}(E_\Delta) & \text{for} \quad E_\Delta = W_{sub} > m_\pi + M_N\,, \\ G_{M1}^{\Delta N}(M_N+m_\pi) & \text{otherwise}\,. \end{cases} \quad (24) $$

It turns out that this onshell treatment for $\widetilde{G}_{M1}^{\Delta\bar{N}}$ is a very good approximation, at least for photodisintegration, compared to the exact calculation, where the arguments $k_{\gamma N}$ and W_{sub} in (24) are treated independently.

C. The nucleonic meson exchange current $J_{eff}^{N[2]\,\mu}(z,\vec{k})$

The matrix element of $J_{eff}^{N[2]\,\mu}(z,\vec{k})$ has the following structure

$$ {}^{(-)}\langle NN;\,\vec{p},\alpha)|P_{\bar{N}}J_{eff}^{N[2]\,\mu}(z,\vec{k})P_{\bar{N}}|d\rangle = \frac{1}{N_d}{}^{(-)}\langle NN;\,\vec{p},\alpha)|P_{\bar{N}}J_{eff}^{N[2]\,\mu}(z,\vec{k})\frac{\hat{R}(z-k)}{\hat{Z}_{[2]}^{os}}P_{\bar{N}}|d\rangle\,, \quad (25) $$

where $J_{eff}^{N[2]\,\mu}(z,\vec{k})$ consists of a static ρ MEC, a retarded π MEC, and a retarded $\gamma\pi\rho/\omega$-current $J^{(diss)\,\mu}(z,\vec{k}\,)$

$$ J_{eff}^{N[2]\,\mu}(z,\vec{k}) = J^{(\rho)\,\mu}(\vec{k}) + J^{(\pi)\,\mu}(z,\vec{k}\,) + J^{(diss)\,\mu}(z,\vec{k}\,)\,. \quad (26) $$

A new feature of retardation is the fact, that above pion threshold the retarded currents can be split into a part containing a pole and a regular part (*nonpole*)

$$ J^{(\pi)/(diss)\,\mu}(z,\vec{k}\,) = J_{pole}^{(\pi)/(diss)\,\mu}(z,\vec{k}\,) + J_{nonpole}^{(\pi)/(diss)\,\mu}(z,\vec{k}\,)\,. \quad (27) $$

The pole part describes the reabsorption of a real pion by a nucleon. Furthermore, the retarded π MEC splits into a contact (c), pion-in-flight (f), vertex (v) and recoil contribution (r)

$$ J^{(\pi)\,\mu}(z,\vec{k}\,) = J^{(\pi)/c\,\mu}(z,\vec{k}\,) + J^{(\pi)/f\,\mu}(z,\vec{k}\,) + J^{(\pi)/v\,\mu}(z,\vec{k}\,) + J^{(\pi)/r\,\mu}(z,\vec{k}\,)\,. \quad (28) $$

A graphical illustration of these currents is given in Fig. 11. In addition, because of the nonvanishing πd interaction V_{XX}^0, currents like those depicted in Fig. 12 would have to be taken into account. However, a detailed analysis has shown that these contributions can be neglected in deuteron photodisintegration. This approximation is realized by the substitution

$$G^X(z) = \left(z - H_{0,XX} - V^0_{XX}\right)^{-1} \longrightarrow G_0(z) = (z - H_{0,XX})^{-1} \tag{29}$$

in the above expressions (see Eq. (49) of I).

Explicitly, one obtains for the various components

$$J^{(\pi)/c\,\mu}_{pole}(z,\vec{k}\,) = \sum_{i,j=1,2;\,j\neq i} v^0_{\bar{N}X_\pi}(j) G_0(z)\, j^{(1)\,\mu}_{X_\pi\bar{N}}(\vec{k},i)\,, \tag{30}$$

$$J^{(\pi)/c\,\mu}_{nonpole}(z,\vec{k}\,) = \sum_{i,j=1,2;\,j\neq i} j^{(1)\,\mu}_{\bar{N}X_\pi}(\vec{k},i)\, G_0(z-k) v^0_{X_\pi\bar{N}}(j)\,, \tag{31}$$

$$\begin{aligned} J^{(\pi)/f\,\mu}_{pole}(z,\vec{k}\,) = \sum_{i,j=1,2;\,j\neq i} \Big(& v^0_{\bar{N}X_\pi}(j) G_0(z)\, j^{(\pi)\,\mu}_{X_\pi X_\pi}(\vec{k})\, G_0(z-k) v^0_{X_\pi\bar{N}}(i) \\ & + v^0_{\bar{N}X_\pi}(j) G_0(z) v^0_{X_\pi X_{\pi\pi}}(i) G_0(z)\, j^{(0)\,\mu}_{X_{\pi\pi}\bar{N}}(\vec{k})\Big)\,, \end{aligned} \tag{32}$$

$$J^{(\pi)/f\,\mu}_{nonpole}(z,\vec{k}\,) = \sum_{i,j=1,2;\,j\neq i} j^{(0)\,\mu}_{\bar{N}X_{\pi\pi}}(\vec{k})\, G_0(z-k) v^0_{X_{\pi\pi}X_\pi}(i) G_0(z-k) v^0_{X_\pi\bar{N}}(j)\,, \tag{33}$$

$$J^{(\pi)/v\,\mu}_{pole}(z,\vec{k}\,) = \sum_{i,j=1,2;\,j\neq i} v^0_{\bar{N}X_\pi}(j) G_0(z)\, j^{(1v)\,\mu}_{X_\pi\bar{N}}(\vec{k},i)\,, \tag{34}$$

$$J^{(\pi)/v\,\mu}_{nonpole}(z,\vec{k}\,) = \sum_{i,j=1,2;\,j\neq i} j^{(1v)\,\mu}_{\bar{N}X_\pi}(\vec{k},i)\, G_0(z-k) v^0_{X_\pi\bar{N}}(j)\,, \tag{35}$$

$$J^{(\pi)/r\,\mu}_{pole}(z,\vec{k}\,) = \sum_{i,j=1,2;\,j\neq i} \Big(v^0_{\bar{N}X_\pi}(j) G_0(z)\, j^{nr,\mu}_{real}(\vec{k},i) v^0_{X_\pi\bar{N}}(i) + v^0_{\bar{N}X_\pi}(i) G_0(z)\, j^{nr,\mu}_{real}(\vec{k},i) v^0_{X_\pi\bar{N}}(j)\Big)\,, \tag{36}$$

$$J^{(\pi)/r\,\mu}_{nonpole}(z,\vec{k}\,) = 0\,, \tag{37}$$

$$\begin{aligned} J^{(diss)\,\mu}_{pole}(z,\vec{k}\,) = \sum_{i,j=1,2;\,j\neq i} \Big(& v^0_{\bar{N}X_\pi}(i) G_0(z)\, j^{(\pi)\,\mu}_{X_\pi X_x}(\vec{k})\, G_0(z-k) v^0_{X_x\bar{N}}(j) \\ & + v^0_{\bar{N}X_\pi}(j) G_0(z) v^0_{X_\pi X_{\pi x}}(i) G_0(z)\, j^{(0)\,\mu}_{X_{\pi x}\bar{N}}(\vec{k})\Big)\Big|_{x\in\{\rho,\omega\}}\,, \end{aligned} \tag{38}$$

$$\begin{aligned} J^{(diss)\,\mu}_{nonpole}(z,\vec{k}\,) = \sum_{i,j=1,2;\,j\neq i} \Big(& j^{(0)\,\mu}_{\bar{N}X_{\pi x}}(\vec{k})\, G_0(z-k) v^0_{X_{\pi x}X_x}(j) G_0(z-k) v^0_{X_x\bar{N}}(i) \\ & + v^0_{\bar{N}X_x}(i) G_0(z)\, j^{(\pi)\,\mu}_{X_x X_\pi}(\vec{k})\, G_0(z-k) v^0_{X_\pi\bar{N}}(j) \\ & + v^0_{\bar{N}X_x}(i) G_0(z) v^0_{X_x X_{\pi x}}(j) G_0(z)\, j^{(0)\,\mu}_{X_{\pi x}\bar{N}}(\vec{k}) \\ & + j^{(0)\,\mu}_{\bar{N}X_{\pi x}}(\vec{k})\, G_0(z-k) v^0_{X_{\pi x}X_\pi}(j) G_0(z-k) v^0_{X_\pi\bar{N}}(i)\Big)\Big|_{x\in\{\rho,\omega\}}\,. \end{aligned} \tag{39}$$

In the present evaluation, we have used a nonrelativistic reduction of the $\pi\bar{N}$ vertex for the sake of simplicity. The bare couplings have to be renormalized, of course, with the renormalization operator $\hat{Z}^{os}_{[2]}$ in (25). Therefore, it is useful to introduce renormalized MECs according to

$$\mathcal{J}^{(\rho)/(\pi)/(diss)\,\mu}(z,\vec{k}\,) = \frac{1}{\hat{Z}^{os}_{[2]}} J^{(\rho)/(\pi)/(diss)\,\mu}(z,\vec{k}\,) \frac{1}{\hat{Z}^{os}_{[2]}}\,, \tag{40}$$

so that the relevant matrix element (25) has the structure

$$\begin{aligned} {}^{(-)}\langle NN;\vec{p},\alpha|P J^{N[2]\,\mu}_{eff}(z,\vec{k}\,)P|d\rangle = \frac{1}{N_d}\, {}^{(-)}\langle NN;\vec{p},\alpha|P_{\bar{N}} \frac{\widehat{Z}^{os}_{[2]}}{\widehat{R}(z)} \Big(& \mathcal{J}^{(\rho)\,\mu}(\vec{k}\,) \\ & + \hat{R}^\pi(z)\left(\mathcal{J}^{(\pi)\,\mu}(z,\vec{k}\,) + \mathcal{J}^{(diss)\,\mu}(z,\vec{k}\,)\right)\hat{R}^\pi(z-k)\Big) P_{\bar{N}}|d'\rangle\,, \end{aligned} \tag{41}$$

where the dressing operator $\hat{R}^\pi$ is neglected in the ρ MEC due to its minor importance.

Summarizing the various contributions to the nucleonic meson exchange currents, we include as retarded currents the π and $\gamma\pi\rho/\omega$ MEC, whereas of the heavier mesons only the ρ MEC will be retained in the static limit. All the other remaining σ, δ, ω, and η MECs are completely neglected in view of their negligible contributions found previously in [21]. Moreover, due to the use of Siegert operators [22] and the much larger mass of the heavy mesons, the role of the corresponding MEC is largely suppressed.

D. The resonant meson exchange current $J_{eff}^{\Delta[2]\,\mu}(z,\vec{k})$

In analogy to the nucleonic MEC, we construct the retarded Δ MEC which is depicted in Figs. 13 and 14. The currents represented in Fig. 13 are the contact, meson-in-flight, vertex, and dissociation contributions to the Δ MEC. In the static limit, they are already taken into account via the static Δ MEC (apart from the dissociation current) so that the problem of double counting arises. In view of the fact that this static Δ MEC leads to a very small contribution in deuteron photodisintegration, it is resonable to assume that retardation will not change this fact qualitatively. Therefore, we take the diagrams of Fig. 13 in the static limit as already contained in the static Δ MEC and consequently set $J_{X\Delta}^{[2]\,\mu}(\vec{k})$ equal to zero.

The recoil contribution of Fig. 14, on the other hand, is not contained in $J_{\Delta\bar{N}}^{[2]\,\mu}(\vec{k})$. Therefore, it is explicitly taken into account. Introducing again renormalized MECs, we obtain for the matrix element of the Δ MEC

$$^{(-)}\langle NN;\,\vec{p},\alpha|P_\Delta J_{eff}^{\Delta[2]\,\mu}(z,\vec{k})P_{\bar{N}}|d\rangle = \frac{1}{N_d}{}^{(-)}\langle NN;\,\vec{p},\alpha|P_\Delta\Big(\mathcal{J}_{\Delta\bar{N}}^{[2]\,\mu}(\vec{k}) + \mathcal{J}_\Delta^{(\pi)/r\,\mu}(z,\vec{k}\,)\hat{R}^\pi(z-k)\Big)P_{\bar{N}}|d'\rangle\,, \tag{42}$$

where the quantities $\mathcal{J}_{\Delta\bar{N}}^{[2]\,\mu}(\vec{k})$ and $\mathcal{J}_\Delta^{(\pi)/r\,\mu}(z,\vec{k}\,)$ are defined in analogy to (40).

E. The effective current operator in the static limit

Until now, we have only considered the *retarded* form of the effective current. In the static case, considerable simplifications occur. Whereas the one-body contributions remain unaltered (apart from the dressing factors which are, of course, not present in static calculations because in this case only physical instead of bare nucleons appear), we have to substitute the retarded meson-NN propagators in Eqs. (30) through (39) by their static limits, i.e.

$$G_0(z) \text{ and } G_0(z-k) \longrightarrow -\frac{1}{h_x}\,, \tag{43}$$

where h_x denotes the kinetic energy of a meson x. Consequently, the pole structure of the MEC is lost. The meson-nucleon vertices in the corresponding expressions are those used in the static Bonn-OBEPR potential [23] so that the sum of the pion-in-flight, vertex and contact MEC fulfils current conservation with the π exchange part V_{OBEPR}^π of the Bonn-OBEPR potential

$$\vec{k}\cdot\Big(\vec{J}_{stat}^{\,\pi/c}(\vec{k}) + \vec{J}_{stat}^{\,\pi/f}(\vec{k}) + \vec{J}_{stat}^{\,\pi/v}(\vec{k})\Big) = \Big[V_{OBEPR}^\pi\,,\,\rho_{real}^{nr}(\vec{k})\Big]\,. \tag{44}$$

Note however, that a static recoil contribution does not appear, because in the static limit the wave function renormalization current cancels exactly the recoil current [24,25]. Likewise, the recoil contribution in the Δ MEC (Fig. 14) has to be neglected, too.

F. Inconsistencies in static approaches

At the end of the discussion of the effective current operator, we would like to point out some inconsistencies in static approaches, namely the fact that the Δ current and the π MEC are *not* independent from each other. From Fig. 15 it becomes evident that the Born terms of the $M_{1+}^{(3/2)}$ amplitude are related to a part of the π MEC in the two-nucleon system, namely to a part of the pion-in-flight and the recoil current. A static treatment of the MEC leads therefore to serious inconsistencies. For example, the crossed nucleon pole graph is not contained in the static π MEC because the respective recoil MEC is not present at all in static approaches due to its cancellation against the wave function renormalization current. How critical this inconsistency is has been demonstrated by Wilhelm *et al.* [12,16] in determining another effective $\gamma\bar{N}\Delta$ coupling, denoted henceforth by $\widetilde{G}_{M1}^{\Delta\bar{N}}$(eff3), in a fit to the data where the Born amplitude in (11) is set equal to zero so that it is contained effectively in this coupling. At least below the resonance position this "modified" coupling is considerably larger as the original coupling (compare the dashed and dotted curves in Fig. 9). In view of this rather large difference between the two couplings, Wilhelm *et al.* [16] had already suspected that retardation in the MEC may become important in the Δ region. Using the modified parameters, a much improved description of the total cross section was achieved (see Sect. VI), though the differential cross section was still poorly described in the Δ region. Moreover, it is obvious that the modified coupling is conceptually not very satisfying because the neglect of the Born amplitude leads formally to a vanishing rescattering amplitude, so that the resulting effective $\gamma\bar{N}\Delta$ coupling is identical to the bare one and therefore energy independent, in contrast to the present parametrization in Eq. (17).

V. THE QUESTION OF GAUGE INVARIANCE

Now, we would like to discuss the question whether the effective current $J^{\mu}_{eff}(z,\vec{k})$ is gauge invariant, i.e., is consistent with the hadronic interaction. As first, we will formulate the continuity equation for the *effective* operators. From the continuity equation for the *full* current operator

$$\langle f|\left(\left[H,J^0(\vec{k})\right]\,-\,\vec{k}\cdot\vec{J}(\vec{k})\right)|i\rangle=0 \tag{45}$$

one obtains straightforwardly the relation

$$\langle f|P\,\vec{k}\cdot\vec{J}_{eff}(z_f,\vec{k})\,P|i\rangle=\langle f|P\left(H_{eff}(z_f)\rho_{eff}(z_f,\vec{k})-\rho_{eff}(z_f,\vec{k})H_{eff}(z_i)\right)P|i\rangle\,, \tag{46}$$

where $z_{i/f}=E_{i/f}\pm i\epsilon$, and the interaction part $V_{eff}(z)$ of the effective Hamiltonian consists of a disconnected and a connected part

$$V_{eff}(z)=V^{dis}_{eff}(z)+V^{con}_{eff}(z)\,, \tag{47}$$

with

$$V^{dis}_{eff}(z)=V^{[c]}_{PP}+\left[V^0_{PX}G_0(z)V^0_{XP}\right]_{dis}\,, \tag{48}$$

$$V^{con}_{eff}(z)=V^{0\,[2]}_{PP}+\left[V^0_{PX}G_0(z)V^0_{XP}\right]_{con}\,. \tag{49}$$

Note that we have neglected V^0_{XX} in V^{con}_{eff} in view of the discussion in Sect. IV C.

Splitting the hadronic interaction and the current into one- and two-body parts, one obtains

$$\langle f|P\,\vec{k}\cdot\vec{J}^{[1]}_{eff}(z_f,\vec{k})P\,|i\rangle=\langle f|P\left[\left(H_{0\,PP}+V^{dis}_{eff}(z_f)\right)\rho^{[1]}_{eff}(z_f,\vec{k})-\rho^{[1]}_{eff}(z_f,\vec{k})\left(H_{0\,PP}+V^{dis}_{eff}(z_i)\right)\right]P\,|i\rangle\,, \tag{50}$$

$$\begin{aligned}\langle f|P\,\vec{k}\cdot\vec{J}^{[2]}_{eff}(z_f,\vec{k})P\,|i\rangle=\langle f|P\Big[&V^{con}_{eff}(z_f)\Big(\rho^{[1]}_{eff}(z_f,\vec{k})+\rho^{[2]}_{eff}(z_f,\vec{k})\Big)\\&-\Big(\rho^{[1]}_{eff}(z_f,\vec{k})+\rho^{[2]}_{eff}(z_f,\vec{k})\Big)V^{con}_{eff}(z_i)\Big]P|i\rangle\,.\end{aligned} \tag{51}$$

These equations serve as starting point for the discussion of gauge invariance. We will restrict ourselves to the pure nucleonic currents and interactions acting solely in $\mathcal{H}_{\bar{N}}$ for the sake of simplicity. Concering the one-body part in (50), it is clear from the very beginning that in retarded calculations, where V^{dis}_{eff} is not zero, gauge invariance cannot exactly be fulfilled. Note that we do not evaluate explicitly the loops in Fig. 4 which enter into $J^{N[1]\,\mu}_{eff}(z,\vec{k})$ as has been discussed in subsection II B. On the other hand, the corresponding loop in V^{dis}_{eff} has to be evaluated due to the requirement of unitarity of the hadronic interaction. Therefore, Eq. (50) is only valid in the onshell case, i.e., for

$$P_{\bar{N}}|i\rangle=|\bar{N}\bar{N};\vec{p}_i,\alpha_i\rangle\,,\quad P_{\bar{N}}|f\rangle=|\bar{N}\bar{N};\vec{p}_f,\alpha_f\rangle\,, \tag{52}$$

where $\vec{p}_{i/f}$ is given by $E_{i/f}=2e^{nr}_N(\vec{p}_{i/f})$. Note that in this case V^{dis}_{eff} is exactly zero. But in static approaches, Eq. (50) can always be fulfilled because of $V^{dis}_{eff}\equiv 0$.

We now turn to the discussion of the two-body part in (51). According to (26), the effective current operator $J^{N[2]\,\mu}_{eff}(z,\vec{k})$ consists of the π and ρ MEC and the $\gamma\pi\rho/\omega$ currents. With respect to the ρ MEC, we refer to the discussion at the end of subsection II B. Concerning the $\gamma\pi\rho/\omega$ contribution, one should notice that the corresponding charge operator vanishes due to the use of nonrelativistic vertex structures, whereas the remaining spatial part $\vec{J}^{(diss)}(z,\vec{k}\,)$ is purely transverse

$$\vec{k}\cdot\vec{J}^{(diss)}(z,\vec{k}\,)=0\,. \tag{53}$$

Consequently, (51) is fulfilled with respect to the dissociation current. The remaining retarded π MEC satisfies ($z_i=z_f-k$)

$$\vec{k}\cdot\vec{J}^{(\pi)}(z_f,\vec{k})=V^{\pi\,con}_{eff}(z_f)\rho^{nr}_{real}(\vec{k})-\rho^{nr}_{real}(\vec{k})V^{\pi\,con}_{eff}(z_i)+kJ^{(\pi)\,0}(z_f,\vec{k})+\mathcal{A}(z_f,\vec{k}\,)+\hat{\mathcal{O}}\left(\frac{1}{M_N^3}\right) \tag{54}$$

with the retarded π exchange potential

$$V_{eff}^{\pi\,con}(z) = \left[V_{\bar{N}X_\pi}^{0\,nonrel}\, G_0(z) V_{X_\pi \bar{N}}^{0\,nonrel} \right]_{con} \tag{55}$$

– note that in (55) $V_{\bar{N}X_\pi}^{0\,nonrel}$ occurs due to the use of the nonrelativistic pion-nucleon vertex in the MEC –, and the auxiliary quantity

$$\begin{aligned}\mathcal{A}(z,\vec{k}\,) = \sum_{i,j=1,2;\, j\neq i} \Big\{ \Big(v_{\bar{N}X_\pi}^{0\,nonrel}(i) G_0(z) v_{X_\pi X_{\pi\pi}}^{0}(j) G_0(z)\, \rho_{X_{\pi\pi}\bar{N}}^{(0)}(\vec{k}) \Big)\ (E_i - H_{0\,\bar{N}\bar{N}}) \\ - (E_f - H_{0\,\bar{N}\bar{N}})\ \Big(\rho_{\bar{N}X_{\pi\pi}}^{(0)}(\vec{k})\, G_0(z-k) v_{X_{\pi\pi}X_\pi}^{0\,nonrel}(i) G_0(z-k) v_{X_\pi \bar{N}}^{0}(j) \Big) \Big\}\ .\end{aligned} \tag{56}$$

In general, only between plane waves the matrixelement of $\mathcal{A}(z,\vec{k}\,)$ vanishes, which fact indicates that in a retarded approach additional MECs of at least fourth order in the pion-nucleon coupling are necessary for ensuring gauge invariance. Examples for such contributions are depicted in Fig. 16. They are quite complicated and beyond the scope of the present work. In the static limit such MECs are not present because they either cancel out each other or cancel against corresponding wave function renormalization currents so that (51) is satisfied.

In summary, gauge invariance is fulfilled up to second order in the meson-nucleon coupling constant, whereas violations appear in higher order. However, we hope that by the use of the Siegert decomposition of the electric multipoles [22] at least a part of these neglected higher order contributions are taken into account implicitly.

VI. RESULTS FOR DEUTERON PHOTODISINTEGRATION

We now will discuss the results for deuteron photodisintegration. The formalism for calculating the various observables may be found in the review [22]. As currents we consider all currents discussed before, i.e., the one-body spin and convection current as well as the spin-orbit current and π and ρ MEC. The parameters of the coupling constants are chosen consistently with the underlying NN interction. We have included all multipoles up to $L \leq 4$. For the electric transitions we have used the Siegert operators [22] which incorporate a large fraction of MEC contributions. They include besides the usual one-body density also two-body charge terms as described in Sect. IV C. The remaining MEC contributions beyond the Siegert operators are evaluated explicitly. In view of the fact, that retardation is most important at short distances, we have considered retardation in the contact, vertex, meson-in-flight and dissociation MECs only for multipoles up to $L \leq 2$, while for $L > 2$ the static expressions are used, which is sufficient as we have checked in detail.

A. Retardation effects in a pure nucleonic model

We will begin the discussion by studying first the influence of retardation in a pure nucleonic model, where the Δ d.o.f. as well as the πd channel are switched off so that only a pure NN interaction and the corresponding currents are taken into account. For the sake of simplicity, the dissociation current is also switched off. In detail, we consider four different types of calculations which differ with respect to static or retarded potentials and MECs, comprising contact, vertex and meson-in-flight currents, and with respect to the recoil MEC. We will denote them by N(potential, current, recoil current), and list the four cases which we consider in Table I. As static potential we use the Bonn OBEPR model, while for the retarded interaction we take the Elster model.

It is obvious that due to the neglect of explicit Δ d.o.f. no realistic description is possible above about $k_{lab} = 100$ MeV. But here we are interested mainly in the relative sensitivity of the cross sections with respect to the various static and retarded approaches. For this reason we show in Fig. 17 only the ratios of the total cross sections with respect to N(stat,stat,0). One readily notices that retardation in the hadronic interaction, i.e., going from N(stat,stat,0) to N(ret,stat,0), leads to a drastic reduction of the cross section which amounts to about 25 percent at $k_{lab} = 240$ MeV. On the other hand, retardation in the meson-in-flight, contact and vertex MECs is almost negligible. It turns out that retardation is important only in the lowest multipole transitions to the $^1S_0$ and $^3P_0$ partial waves, which are of minor importance in the total cross section, except directly at threshold. In general, the influence of retardation in the MEC decreases rapidly with increasing multipole order. On the other hand, the recoil current contribution turns out to be very important as is evident comparing N(ret,ret,0) with N(ret,ret,1) in Fig. 17. It is of particular importance in the contributions of the $^1D_2$ and $^3F_2$ partial waves.

In summary, it turns out that below π threshold, the static and the full retarded calculations predict the same cross section within a few percent. This result is at variance with the previous work of Schmitt *et al.* [26], in which retardation in potential and current had been considered using a p/M_N expansion below π threshold. A sizeable

decrease of the cross section was found in retarded calculations compared to a static approach. In contrast to the present work, also the wave function renormalization current was included but no renormalization of the continuum wave functions was applied. Only the bound deuteron wave function had been renormalized globally by a constant. In a correct approach, however, the wave function renormalization current should have been left out as well as the renormalization of the deuteron state. This erroneous treatment lead to the mentioned decrease of the cross section.

In the energy region above π threshold, the equivalence between static and retarded frameworks breaks down, the difference increasing with increasing energy as can be seen in Fig. 17. This is not surprising, because above π threshold the pion can become an onshell particle which fact is only taken into account by the retarded πNN propagators, whereas for a static framework no coupling between the NN and the open πNN channel is possible, i.e., retarded and static approaches exhibit a different behaviour.

B. Retardation effects in the Δ resonance region

Now we will turn to the energy region of the Δ resonance, applying our full model which includes explicitly Δ degrees of freedom. In detail, we will consider four different static and five different retarded approaches whose nomenclature is explained in Tables II and III. The corresponding hadronic interaction models are described in detail in I and are therefore not repeated in this paper. We have restricted the full inclusion of Δ d.o.f. to partial waves with total angular momentum $j \leq 3$, and use for $j \geq 4$ – similar to [16] – the impulse approximation [27] in which the $N\Delta$ components are given in first order perturbation theory by

$$P_\Delta |NN; \vec{p}, \alpha\rangle^{(-)} = G_0^{(\Delta)}(z)\, V^{con}_{[2]\,\Delta\bar{N}}(z) P_{\bar{N}} |NN; \vec{p}, \alpha\rangle^{(-)}\,, \tag{57}$$

where the nucleonic component $|NN; \vec{p}, \alpha\rangle^{(-)}$ is obtained in pure nucleonic space from a realistic NN potential.

As first we consider the results of the static MEC cases in Figs. 18 and 19. The model CC(stat1), which has already been used by Wilhelm *et al.* [16], shows the already mentioned significant underestimation of the total cross section by about 30 % at $k_{lab} = 260$ MeV. Moreover, above $k_{lab} = 300$ MeV the differential cross sections develop a dip structure around 90° in clear contradiction to the experimental data. Due to the slightly stronger $\gamma\bar{N}\Delta$ coupling in the model CC(stat2) – compare the couplings $\widetilde{G}^{\Delta\bar{N}}_{M1}$(eff 1) and $\widetilde{G}^{\Delta\bar{N}}_{M1}$(eff 2) in Fig. 9 – this model leads to a noticeable enhancement of σ_{tot} which is, however, not sufficient to bridge the gap to experiment. The additional improvements, in the approach CC(stat3), especially the incorporation of the $\gamma\pi\rho/\omega$ currents, lead to a further enhancement of the cross section for $k_{lab} \lesssim 340$ MeV. Compared to the recent Mainz data [28], the theoretical underestimation of σ_{tot} amounts to not more than 10 % at $k_{lab} = 260$ MeV but increases to about 40 % at $k_{lab} = 440$ MeV. Moreover, the dip problem in the differential cross section has not been resolved. The last static model CC(stat4) shows, as has already been discussed in [16], a rather good description of the total cross section in the peak region due to the substantially stronger $\gamma\bar{N}\Delta$ coupling, but again the dip problem as well as the underestimation of the cross section at higher energies remains. Moreover, as has been stressed in Sect. IV F, this approach is quite unsatisfactory from a conceptual point of view.

The results for the retarded current models are shown in Figs. 20 and 21. The effect of introducing retardation in the hadronic interaction but keeping the currents still static can be seen by comparing CC(stat3) with CC(ret4). One readily notes a drastic decrease of the cross section. This fact has been noted already for the pure nucleonic case discussed in the previous subsection. Switching on in addition retardation in the currents (transition CC(ret4) $\rightarrow$ CC(ret2)) leads, however, to a drastic increase which overcompensates the reduction of the cross section by the retardation in the hadronic interaction. It turns out that within about 10 % an overall satisfactory description of the total cross section over the whole energy region is achieved. Concerning the differential cross sections, apart from energies below the resonance maximum, the description of the experimental data is almost quantitative, too. Especially the above mentioned dip structure occurring in the static treatment vanishes *completely*. This is mainly due to the additional consideration of the N-Δ-mass difference in $V^0_{N\Delta}$ and $V^0_{\Delta\Delta}$, and due to the recoil current contributions. On the other hand, similar to the pure nucleonic case, retardation in the pion-in-flight, vertex, contact as well as in the dissociation currents is negligible in the total and differential cross sections. With respect to the influence of the πd channel, it turns out that this mechanism leads to a noticeable enhancement below about $k_{lab} = 300$ MeV. This result is at variance with the results of Tanabe and Ohta [29] who found a decrease of σ_{tot} when they incorporated the πd channel. On the other hand, the influence of the πd channel on the $^1D_2$ channel is qualitatively the same than in our approach. Thus, the reason for this difference is unclear.

As next topic, we discuss in Fig. 22 the influence of the parameter $\alpha_{\Delta N\rho}$ describing the additional $\rho N\Delta$ coupling in Eq. (76) of I. Comparing the results of CC(ret1), CC(ret2) and CC(ret3), which differ by the value of $\alpha_{\Delta N\rho}$, but which are equivalent concerning the description of the $^1D_2$ channel in NN scattering, it turns out that the value of $\alpha_{\Delta N\rho}$ is

of considerable importance for energies above about $k_{lab} = 380$ MeV. But similar to NN scattering, an optimal value for $\alpha_{\Delta N\rho}$ could not be determined because of the rather large differences between the different experimental data sets at higher energies [28,30].

Finally, we discuss a few polarization observables. At first, we will consider the linear photon asymmetry Σ for which new experimental data is available [31,32]. In Fig. 23, the results for the approaches CC(stat3), CC(ret4) and CC(ret2) are depicted. The static approach CC(stat3) yields quite a good description for energies up to about $k_{lab} = 300$ MeV. For higher energies, however, an oscillatory structure appears which vanishes completely if retardation in the hadronic interaction is switched on (CC(stat3) $\rightarrow$ CC(ret4)). Moreover, Σ decreases drastically with increasing photon energy. The additional inclusion of retardation in the currents (CC(ret4) $\rightarrow$ CC(ret2)) leads to an overall reduction of Σ except for the highest energy for which a significant change of the shape appears. Compared to the experimental data one finds a satisfactory overall description of the qualitative features. But one notes also some significant deviations around 90°, where theory predicts an asymmetry considerably smaller than experiment. This is particularly significant at $k_{lab} = 220$ MeV in view of the small error bars, while for higher energies the larger errors make the deviations less significant. It is interesting to note that for $k_{lab} = 220$ MeV also the differential cross section exhibits around 90° a sizeable deviation of the theory by about 10 %.

Finally, we show in Figs. 24 and 25 the proton and neutron polarization, respectively. At $k_{lab} = 240$ MeV, the different approaches yield very similar results which are also in good agreement with the experimental data. At $k_{lab} = 400$ MeV hadronic retardation results in a strong overall decrease of the polarization for both neutron and proton (transition CC(stat3) $\rightarrow$ CC(ret4)). Switching on the current retardation leads however to a strong polarization increase in the forward and backward direction while around 90° the polarization is much less affected. This feature is clearly at variance with the few proton polarization data. Due to the fact that in general polarization observables are more sensitive to small reaction mechanisms, one reason for this failure may be the fact that apart from the dominant $^1D_2$ channel several other partial waves (for example the P- and the $^3F_3$ waves) are described only fairly well within the present model (see I for further details). Thus, one has to await future improvements of the hadronic interaction model in order to see whether this failure could be resolved. Certainly, more data of higher accuracy are needed in addition.

VII. SUMMARY AND OUTLOOK

In this paper we have presented the electromagnetic part of a model which is able to incorporate complete retardation in the two-body π MEC and thus is suited for the study of electromagnetic reactions in the two-nucleon sector above pion threshold up to about 500 MeV excitation energy. The electromagnetic current of the hadronic system comprises the nucleonic one-body currents, the Δ excitation and meson exchange currents. The electromagnetic excitation of the Δ resonance has been fixed by fitting the $M_{1+}^{(3/2)}$ multipole of pion photoproduction. Within the present framework, it is possible to construct the necessary retarded π MEC as an effective two-body current operator. In this context we would like to emphasize, that we do not use any wave function renormalization [24], because this procedure is applicable in retarded models only for energies below the π threshold. Consequently, recoil contributions besides the meson-in-flight, vertex and contact MEC have been taken into account in addition. The retarded π MEC is, however, only partially consistent to the corresponding retarded NN interaction. This is mainly due to the neglect of – technically very complicated – MEC of at least fourth order in the πNN coupling constant which are not present in static approaches. On the other side, due to the use of the Siegert operators for the electric multipoles, such explicitly neglected mechanisms are at least partially taken into account. We furthermore would like to emphasize that in the present model *all* free parameters are fixed in advance before studying electromagnetic reactions on the two-nucleon system. In order to test the quality of the developed framework, we have studied photodisintegration of the deuteron, where until now serious problems existed in the theoretical description above π threshold. While below π threshold, say up to about 100 MeV, both frameworks, static and retarded, are equivalent, this equivalence, however, breaks down when approaching π threshold and even more so above, e.g., the total cross section in the retarded framework is considerably enhanced compared to the one in the static framework. Within about 10 %, we obtain a satisfacory description of the experimental data over the whole energy region of the Δ resonance. This improvement is the combined result of various additional independent mechanisms beyond the ones already considered in [16]. These additional ingredients comprise besides the very important retardation effects the dissociation currents, the πd channel and the explicit evaluation of the rescattering amplitude in fixing the $\gamma\bar{N}\Delta$ coupling. Furthermore, also the theoretical description of the differential cross section is considerably improved. Thus, for the first time a model is available which is able to describe the total as well as the differential cross section up to about $k_{lab} = 450$ MeV. However, some problems in desribing the linear photon asymmetry as well as the proton polarization at higher energies are still present.

[1] M. Schwamb and H. Arenhövel, nucl-th/9912017, submitted to Nucl. Phys. A
[2] M. Schwamb, H. Arenhövel, P. Wilhelm, and Th. Wilbois, Phys. Lett. B **420**, 255 (1998)
[3] M. Schwamb, PhD Thesis, Mainz 1999
[4] A. Cambi, B. Mosconi, and P. Ricci, Phys. Rev. Lett. **48**, 462 (1982).
[5] P. Wilhelm, W. Leidemann, and H. Arenhövel, Few-Body Sys. **3**, 111 (1988).
[6] K. M. Schmitt, PhD Thesis, Mainz 1986.
[7] R. M. Davidson, N. C. Mukhopadhyay, and R. S. Wittman, Phys. Rev. D **43**, 71 (1991).
[8] O. Dumbrajs, R. Koch, H. Pilkuhn, G. C. Oades, H. Behrens, J. J. de Swart, and P. Kroll, Nucl. Phys. B **216**, 277 (1983).
[9] M. I. Levchuk, Few-Body Syst. **19**, 77 (1995).
[10] H. J. Weber and H. Arenhövel, Phys. Rep. **36**, 277 (1978).
[11] K.-M. Schmitt, P. Wilhelm, H. Arenhövel, A. Cambi, B. Mosconi, and P. Ricci, Phys. Rev. C **41**, 841 (1990).
[12] P. Wilhelm, PhD Thesis, Mainz 1992.
[13] H. Tanabe and K. Ohta, Phys. Rev. C **31**, 1876 (1985).
[14] R. A. Arndt *el al.*, program SAID.
[15] K. Watson, Phys. Rev. **95**, 277 (1954).
[16] P. Wilhelm and H. Arenhövel, Phys. Lett. B **318**, 410 (1993).
[17] J. H. Koch and E. J. Moniz, Phys. Rev. C **27**, 751 (1983).
[18] J. H. Koch, E. J. Moniz, and N. Ohtsuka, Ann. of Phys. **154**, 99 (1984).
[19] F. A. Berends and A. Donnachie, Nucl. Phys. B **84**, 342 (1975).
[20] H. Göller and H. Arenhövel, Few-Body Sys. **13**, 117 (1992).
[21] F. Ritz, H. Arenhövel, and T. Wibois, Few-Body Syst. **24**, 123 (1998).
[22] H. Arenhövel and M. Sanzone, Photodisintegration of the Deuteron, Few-Body Syst., Supp. **3**, 1 (1991).
[23] R. Machleidt, K. Holinde, and Ch. Elster, Phys. Rep. **149**, 1 (1987)
[24] M. Gari and H. Hyuga, Z. Phys. **277**, 291 (1976)
[25] H. Arenhövel, Czech. J. Phys. **43**, 207 (1993)
[26] K.-M. Schmitt and H. Arenhövel, Few-Body Syst. **7**, 95 (1989)
[27] H. Arenhövel, M. Danos, and H.T. Williams, Nucl. Phys. A **162**, 12 (1971).
[28] R. Crawford *et al.* , Nucl. Phys. A **603**, 303 (1996)
[29] H. Tanabe and K. Ohta, Phys. Rev. C **40**, 1905 (1989).
[30] J. Arends *et al.* , Nucl. Phys. A **412**, 509 (1984)
[31] G. Blanpied *et al.* , Phys. Rev. C **52**, R455 (1995)
[32] S. Wartenberg *et al.* , Few-Body Syst. **26**, 213 (1999).
[33] F. Adamian *et al.* , J. Phys. G **17**, 1189 (1991)
[34] A. S. Bratashevskii, A.I. Derebchinskii, A. A. Zybalov, O. T. Konovalov, P. V. Sorokin and A. E. Tenishev, Sov. J. of Nucl. Phys. **32**, 216 (1980).
[35] F. F. Liu, D. E. Lundquist and B. H. Wiik, Phys. Rev. **165**, 1478 (1968)
[36] H. Ikeda, I. Arai, H. Fujii, T. Fujii, H. Iwasaki, N. Kajiura, T. Kamae, K. Nakamura, T. Sumiyoshi and H. Takeda, Phys. Rev. Lett. **42**, 1321 (1979)
[37] M. Hugi *et al.* , Nucl. Phys. A **472**, 701 (1987)

TABLE I. Nomenclature for the pure nucleonic approaches of Sect. VI A.

notation	potential	MEC	recoil current
N(stat,stat,0)	OBEPR	static	not included
N(ret,stat,0)	Elster	static	not included
N(ret,ret,0)	Elster	retarded	not included
N(ret,ret,1)	Elster	retarded	included

TABLE II. Nomenclature for the *static* models of the coupled channel approach of Sect. VI B. The nomenclature for the hadronic model follows Ref. [1]. The recoil current is always not included.

notation	hadronic model	MEC	$\gamma\bar{N}\Delta$ coupling	$J^{(diss)\ \mu}$
CC(stat1)	CC(stat1,π)	static	$\widetilde{G}_{M1}^{\Delta N}$(eff 2)	not included
CC(stat2)	CC(stat2,π)	static	$\widetilde{G}_{M1}^{\Delta\bar{N}}$(eff 1)	not included
CC(stat3)	CC(stat,π,ρ,0)	static	$\widetilde{G}_{M1}^{\Delta\bar{N}}$(eff 1)	included
CC(stat4)	CC(stat1,π)	static	$\widetilde{G}_{M1}^{\Delta\bar{N}}$(eff 3)	not included

TABLE III. Nomenclature for the various *retarded* models of the coupled channel approach of Sect. VI B. The nomenclature for the hadronic model follows Ref. [1]. In all cases, the $\gamma\bar{N}\Delta$ coupling $\widetilde{G}_{M1}^{\Delta\bar{N}}$(eff 1) has been used. Except for CC(ret4), the retarded recoil current is always included.

notation	hadronic model	MEC	remarks
CC(ret1)	CC(ret,π,ρ,-1)	retarded	
CC(ret2)	CC(ret,π,ρ,0)	retarded	
CC(ret3)	CC(ret,π,ρ,1)	retarded	
CC(ret4)	CC(ret,π,ρ,0)	static	$J^{(\pi)/r}$, $J_{\Delta}^{(\pi)/r}$ not included
CC(ret5)	CC(ret,π,ρ,0)	retarded	πd channel not included

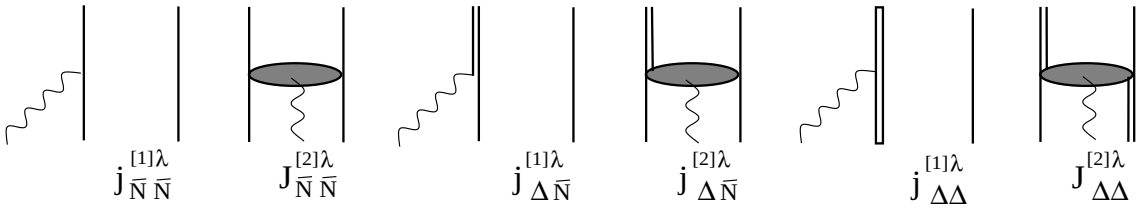

FIG. 1. Diagrammatic representation of the baryonic currents. A shaded ellipse symbolizes a two-body exchange current.

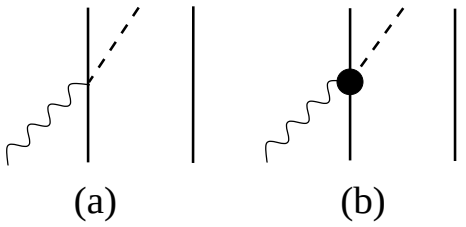

FIG. 2. Diagrammatic representation of the meson production currents $J^{\mu}_{X\bar{N}}$: (a) contact current $j^{(1)\,\mu}_{X\bar{N}}$ and (b) vertex current $j^{(1v)\,\mu}_{X\bar{N}}$.

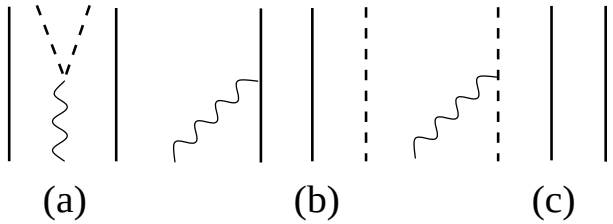

FIG. 3. Diagrammatic representation of the two-meson production current $j^{(0)\,\mu}_{X\bar{N}}$ (a) and the current components J^{μ}_{XX}: (b) nucleon current $j^{\bar{N}\,\mu}_{XX}(\vec{k})$, (c) meson current $j^{X\,\mu}_{XX}(\vec{k})$.

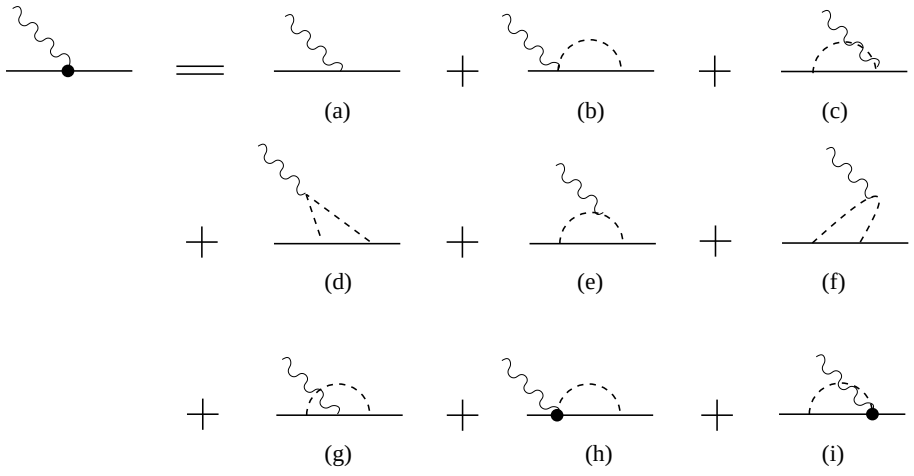

FIG. 4. Diagrammatic representation of the separate contributions to the *physical* one-nucleon current, represented in contrast to the bare nucleon current by a filled circle: (a) bare nucleon current, (b) and (c) contact current, (d) - (f) meson-in-flight current, (g) bare nucleon current with meson in flight, (h) and (i) vertex current.

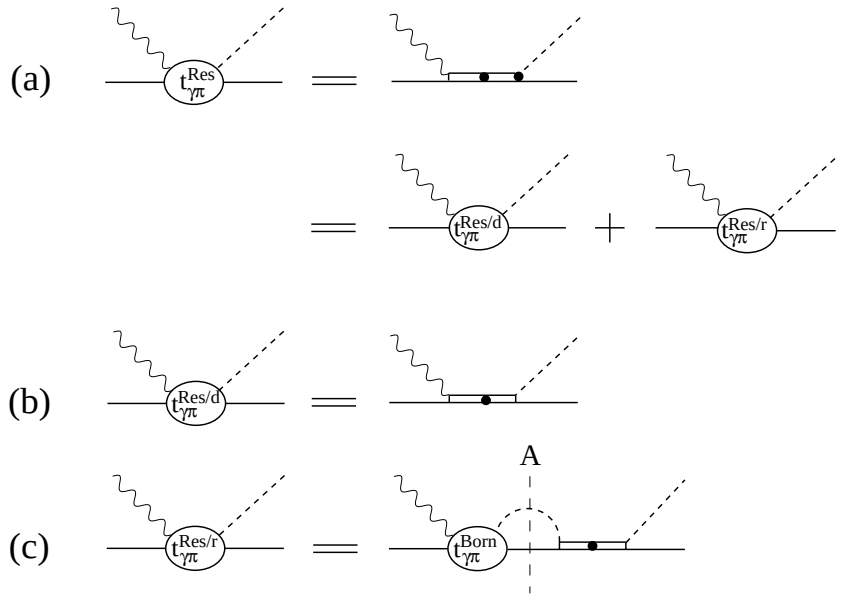

FIG. 5. Diagrammatic representation of the resonant amplitude of pion photoproduction (a) consisting of a direct amplitude (b), and a rescattering contribution (c).

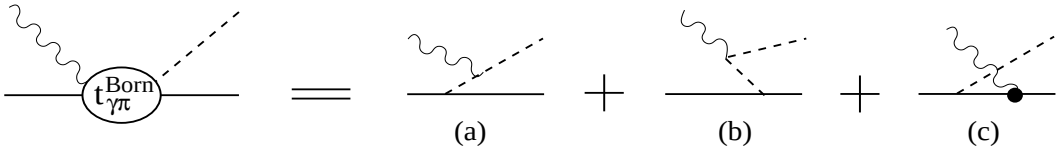

FIG. 6. Diagrammatic representation of the Born amplitude $t^{Born}_{\pi\gamma\,\mu}(z)$ in the $M_{1+}(3/2)$-multipole amplitude. The separate diagrams are denoted as follows: time ordered pion pole terms (a) and (b) and crossed nucleon pole term (c).

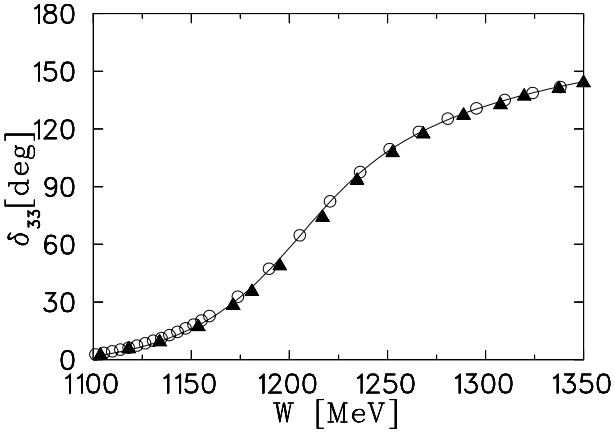

FIG. 7. Experimental P_{33}-scattering phase δ_{33} of πN scattering (triangles from [14], solution SM95) and photoproduction phase $\delta_{M^{(3/2)}_{1+}}$ (open circles from [14], solution SM97K). The solid curve represents our fit using the values of Eq. (67) in I, in which both data sets are considered with equal weight.

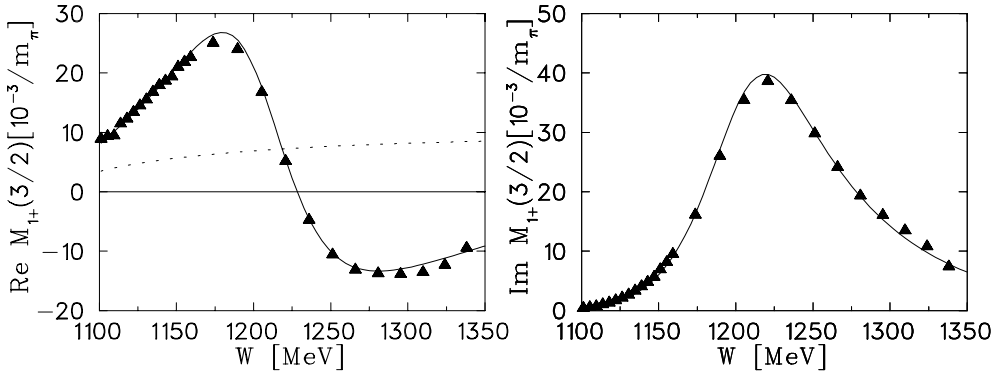

FIG. 8. Fit of the real and the imaginary part of the $M_{1+}^{(3/2)}$ multipole amplitude to the experimental data from [14], solution SM97K. The dotted curve represents the contribution of the Born amplitude.

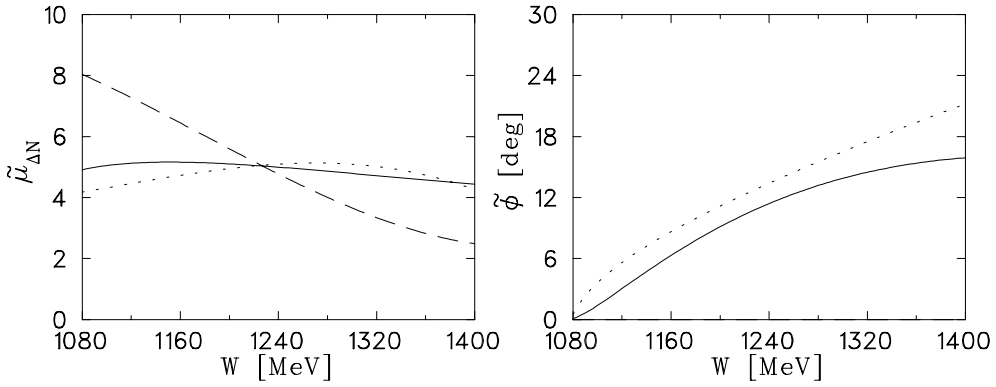

FIG. 9. Energy dependence of the effective $\gamma\bar{N}\Delta$ coupling for the onshell-case $W = e_N^{nr}(\vec{k}) + k$. The left panel shows the modulus $\widetilde{\mu}_{\Delta\bar{N}}(W,k)$ and the right panel the phase $\widetilde{\Phi}(W,k)$. The full curve represents the coupling $\widetilde{G}_{M1}^{\Delta\bar{N}}$(eff1) in (13), and the dotted curve the one of Wilhelm $\widetilde{G}_{M1}^{\Delta\bar{N}}$(eff2) (see (18)). The dashed curve shows the "modified" coupling of Wilhelm *et al.* $\widetilde{G}_{M1}^{\Delta\bar{N}}$(eff3) (see the discussion in Sect. IV F).

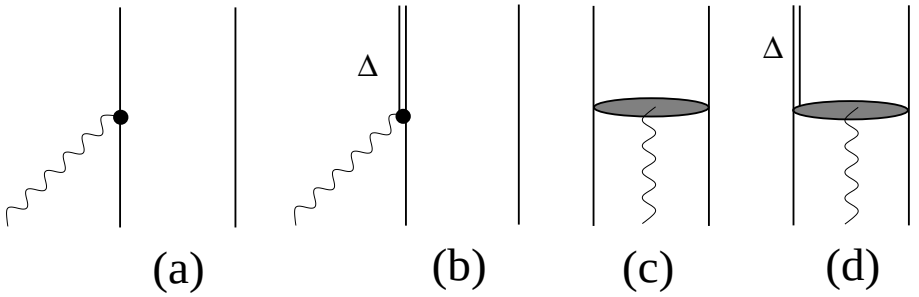

FIG. 10. Diagrammatic representation of the separate contributions to the effective current operator $J_{eff}^{\mu}(z,\vec{k})$ (see Eq. (20)): (a) $J_{eff}^{N[1]\,\mu}(z,\vec{k})$, (b) $J_{eff}^{\Delta[1]\,\mu}(z,\vec{k})$, (c) $J_{eff}^{N[2]\,\mu}(z,\vec{k})$, and (d) $J_{eff}^{\Delta[2]\,\mu}(z,\vec{k})$.

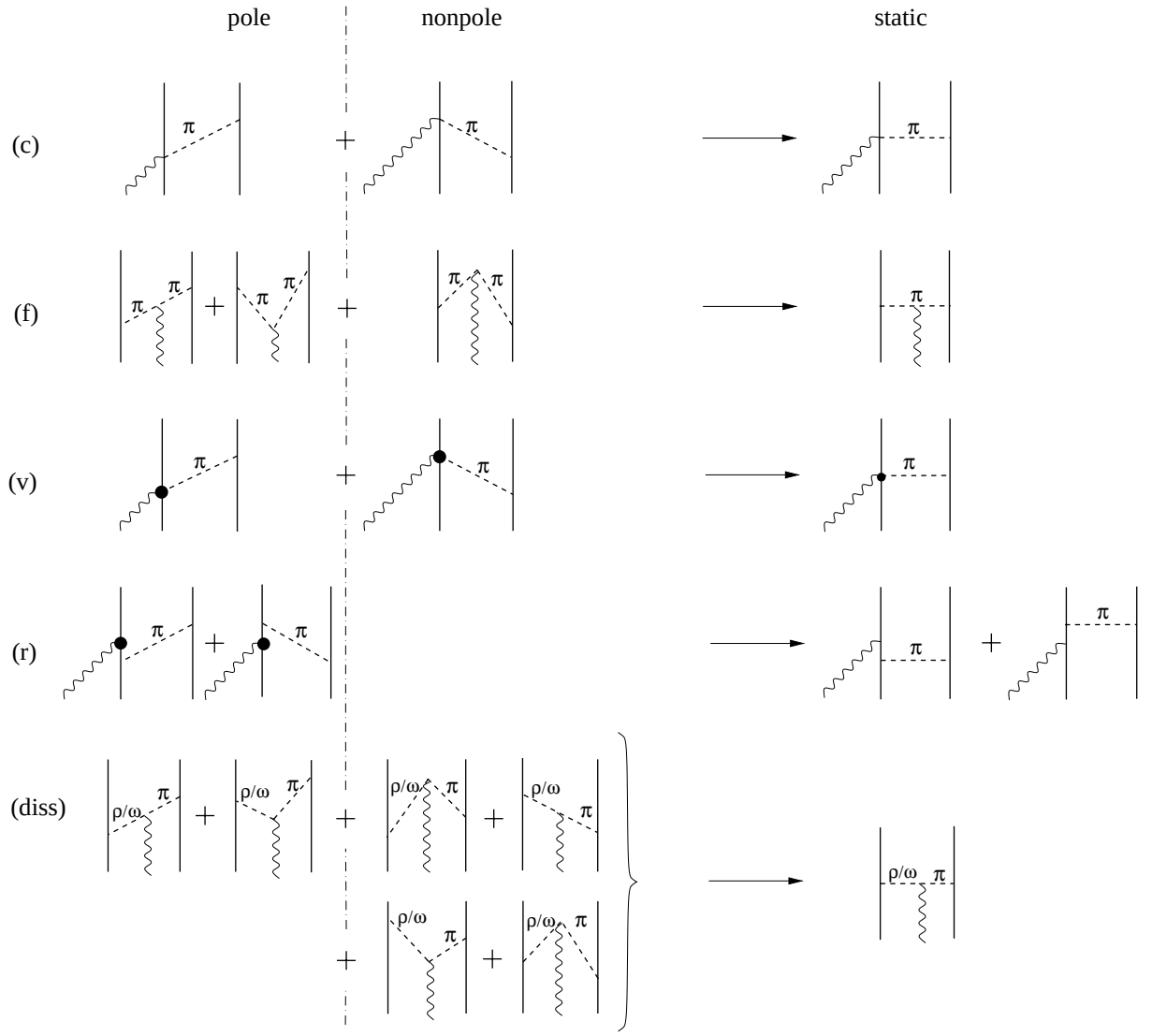

FIG. 11. Diagrammatic representation of the retarded π (contact (c), pion-in-flight (f), vertex (v), recoil (r)) and $\gamma\pi\rho/\omega$ MEC (diss). The arrows indicate the static limit.

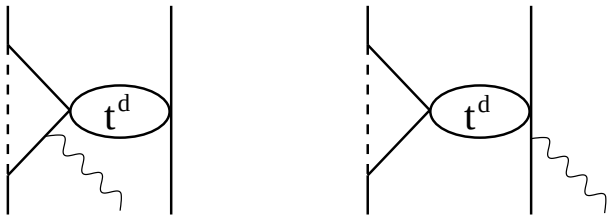

FIG. 12. Examples for effective exchange currents, which are neglected due to the substitution (29).

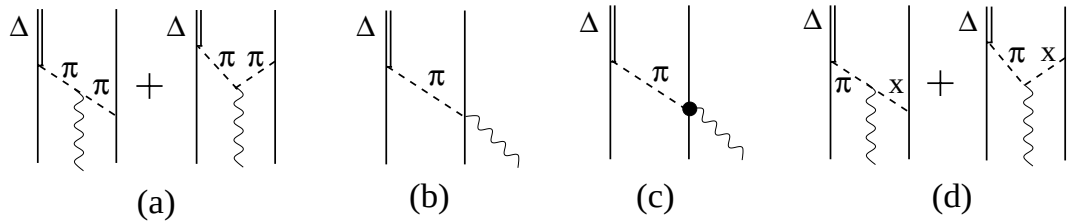

FIG. 13. Diagrammatic representation of the retarded Δ MEC: (a) meson-in-flight, (b) contact, (c) vertex, and (d) dissociation contributions ($x \in \{\rho, \omega\}$).

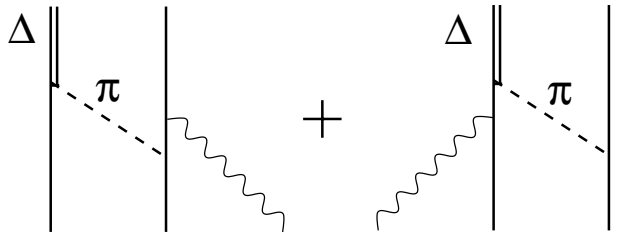

FIG. 14. Diagrammatic representation of the retarded Δ recoil MEC $J_{\Delta}^{(\pi)/r\,\mu}(z, \vec{k}\,)$.

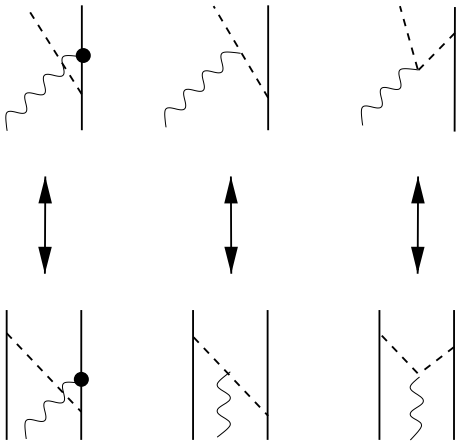

FIG. 15. Correspondence of Born terms of pion photoproduction to π MEC.

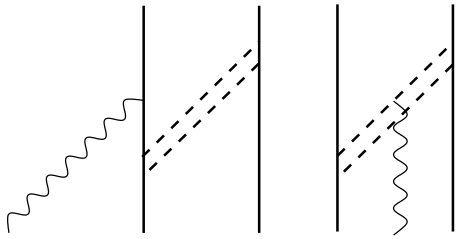

FIG. 16. Diagrammatic representation of retarded MECs which are of fourth order in the pion-nucleon coupling constant.

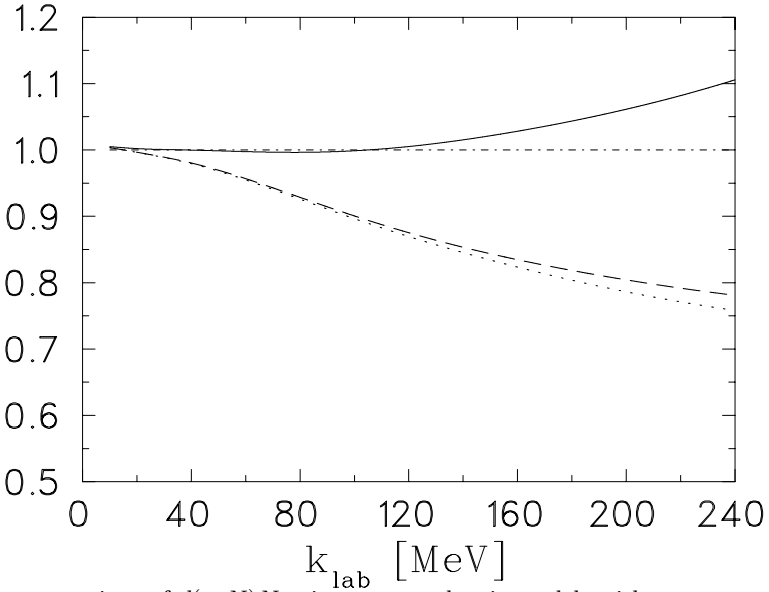

FIG. 17. Ratios of total cross sections of $d(\gamma, N)N$ using pure nucleonic models with respect to σ_{tot}(N(stat,stat,0)): dotted curve: N(ret,stat,0), dashed curve: N(ret,ret,0), full curve: N(ret,ret,1).

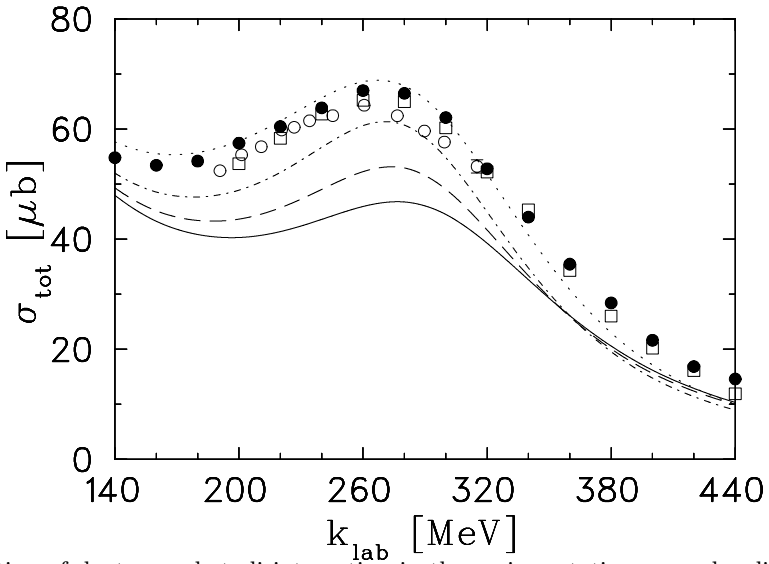

FIG. 18. Total cross section of deuteron photodisintegration in the various static approaches listed in Table II: full curve CC(stat1), dashed curve CC(stat2), dash-dotted curve CC(stat3), and dotted curve CC(stat4). Experimental data from [28] (•), [30] (□) and [31] (○).

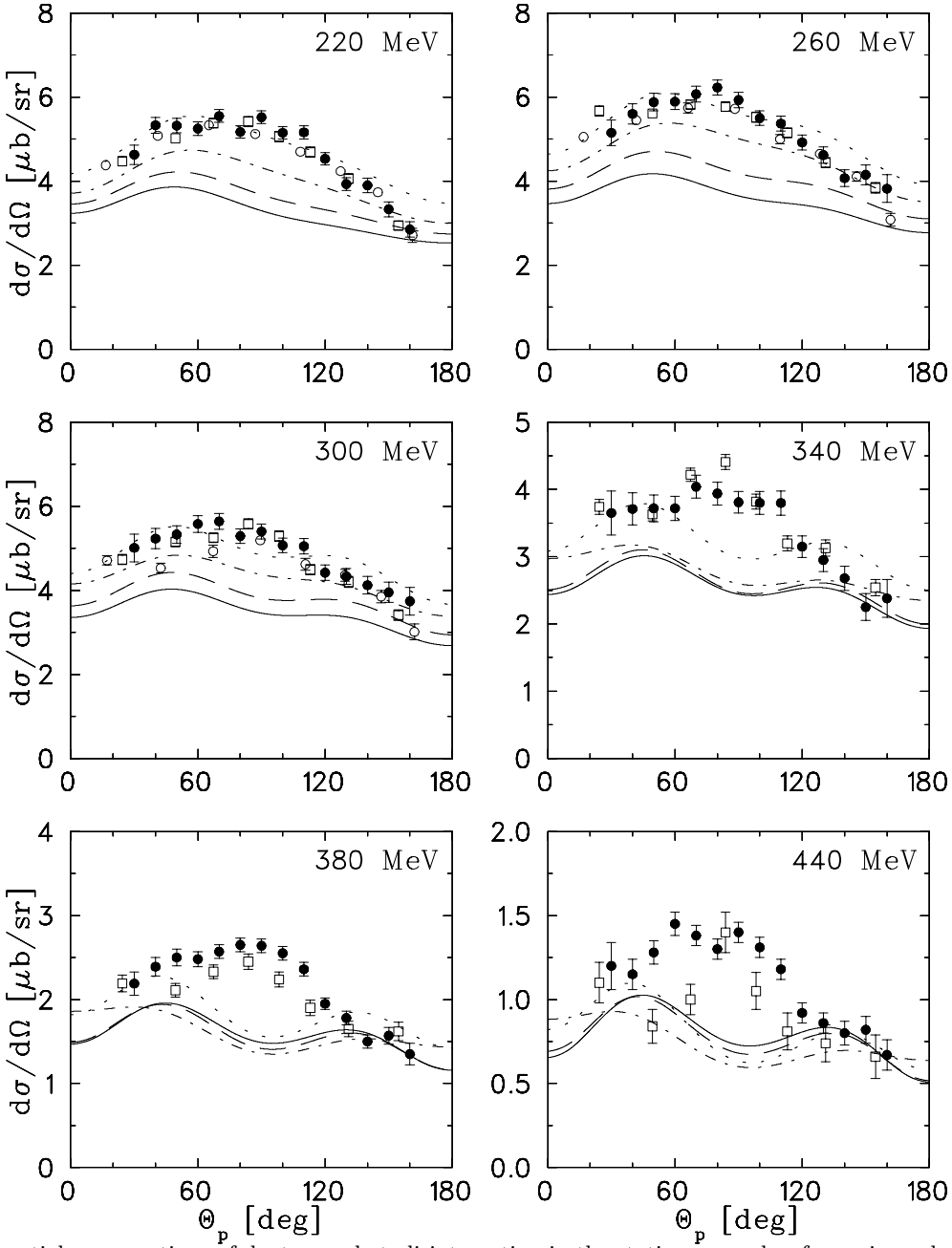

FIG. 19. Differential cross sections of deuteron photodisintegration in the static approaches for various photon energies k_{lab} as function of the c.m. proton angle θ_p. Notation of the curves and experimental data as in Fig. 18.

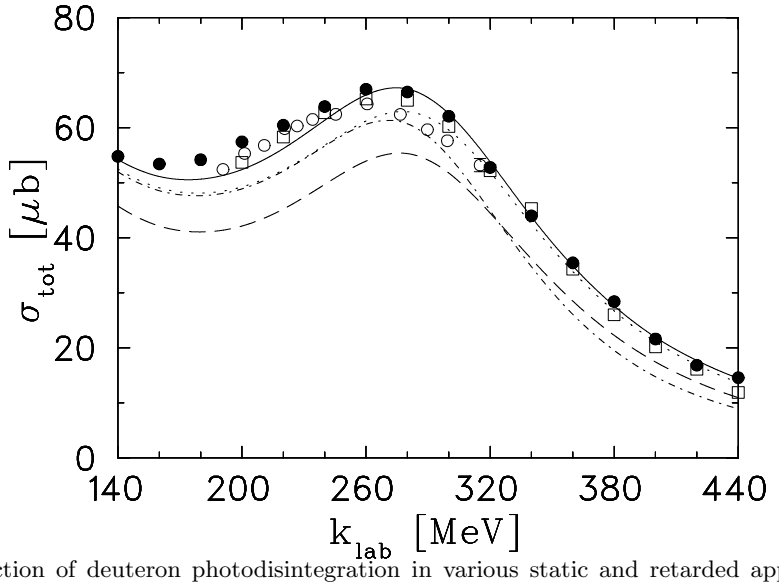

FIG. 20. Total cross section of deuteron photodisintegration in various static and retarded approaches. Notation of the curves (see Tables II and III for the nomenclature): dash-dotted CC(stat3), dashed curve CC(ret4), full curve CC(ret2), dotted curve CC(ret5). Experimental data as in Fig. 18.

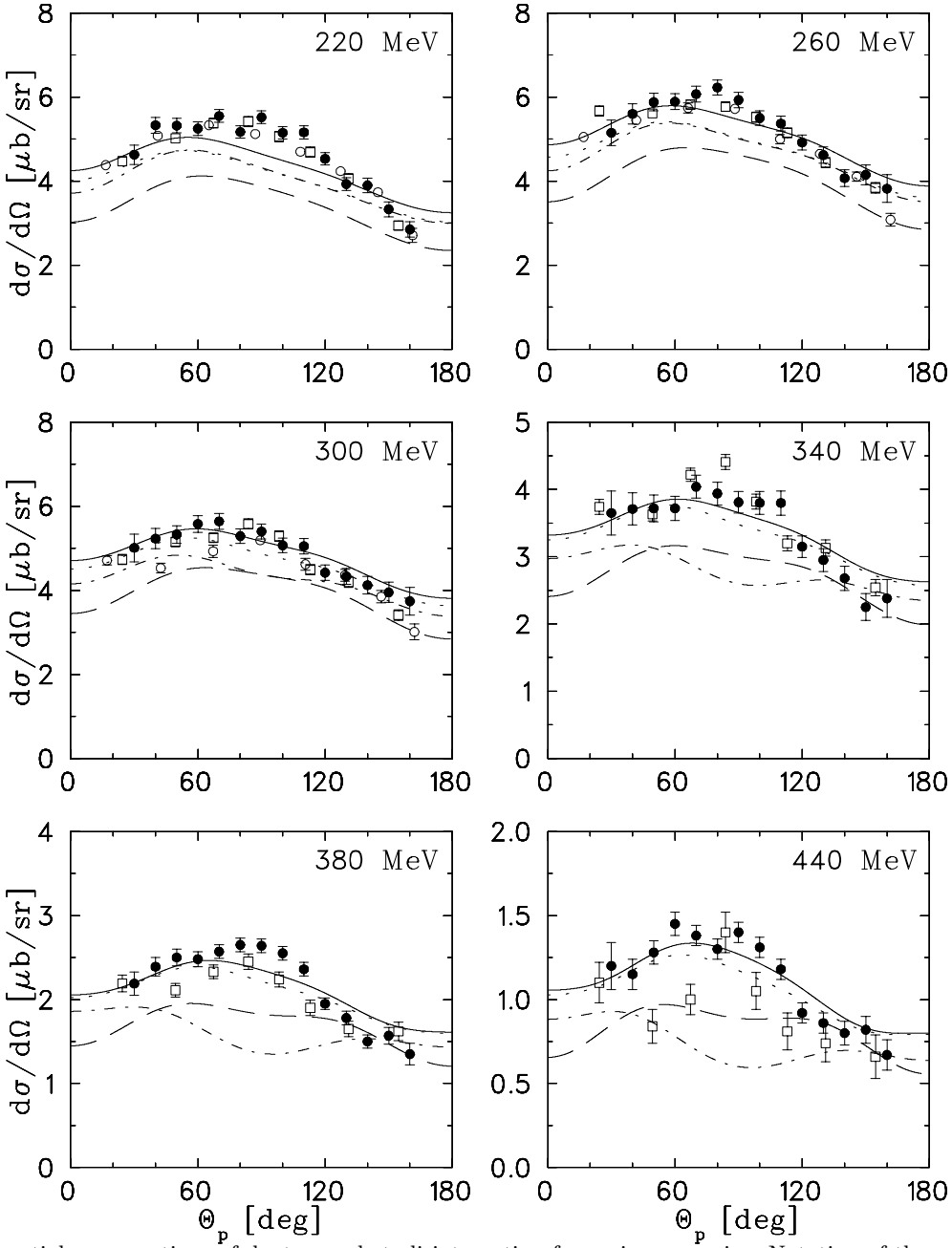

FIG. 21. Differential cross sections of deuteron photodisintegration for various energies. Notation of the curves and experimental data as in Fig. 20.

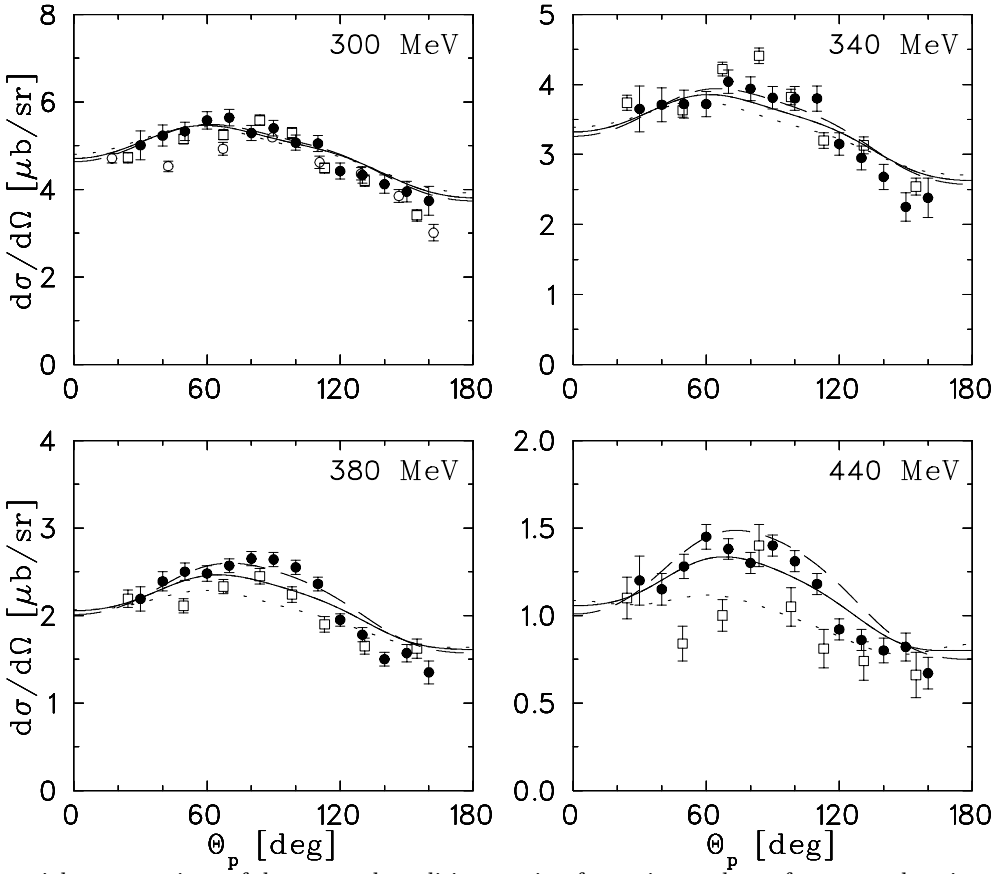

FIG. 22. Differential cross sections of deuteron photodisintegration for various values of $\alpha_{\Delta N\rho}$ and various photon energies. Notation of the curves: dashed curve CC(ret1), full curve CC(ret2), dotted curve CC(ret3). Notation of the experimental data as in Fig. 18.

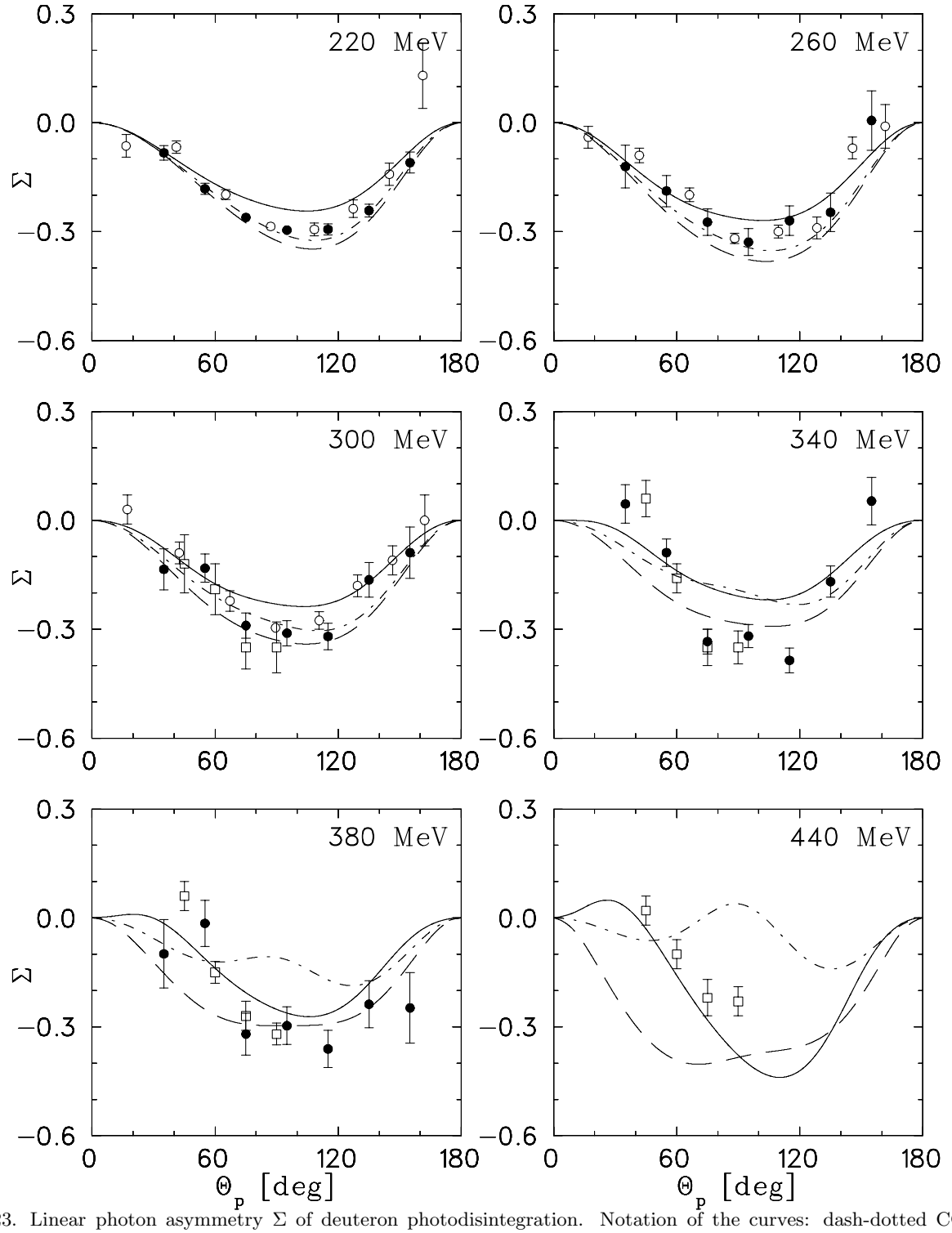

FIG. 23. Linear photon asymmetry Σ of deuteron photodisintegration. Notation of the curves: dash-dotted CC(stat3), dashed CC(ret4), full CC(ret2). Experimental data from [31] (○), [32] (●) and [33] (□).

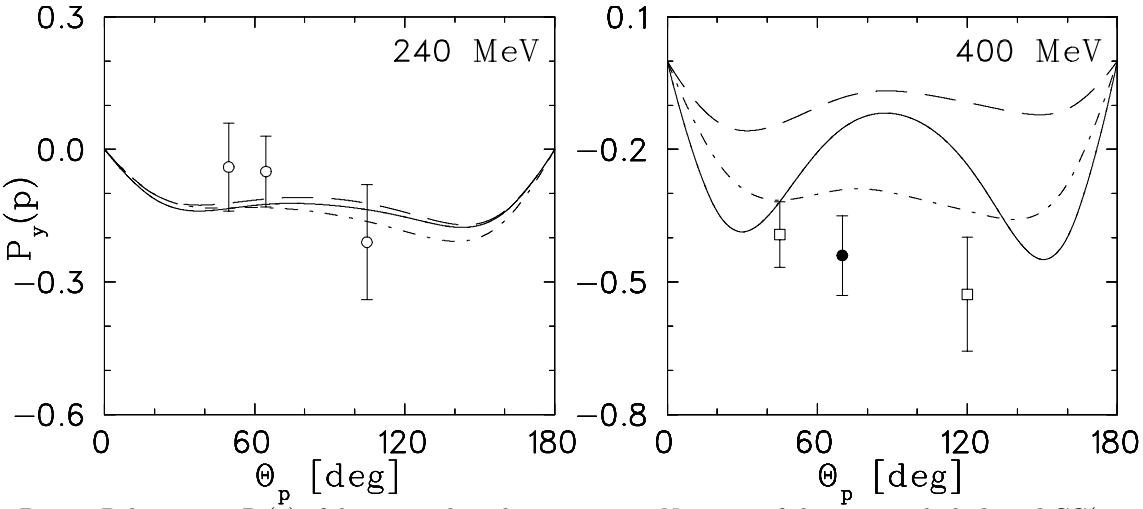

FIG. 24. Proton Polarization $P_y(p)$ of deuteron photodisintegration. Notation of the curves: dash-dotted CC(stat3), dashed CC(ret4), full CC(ret2). Experimental data from [34] (□), [35] (○), and [36] (●).

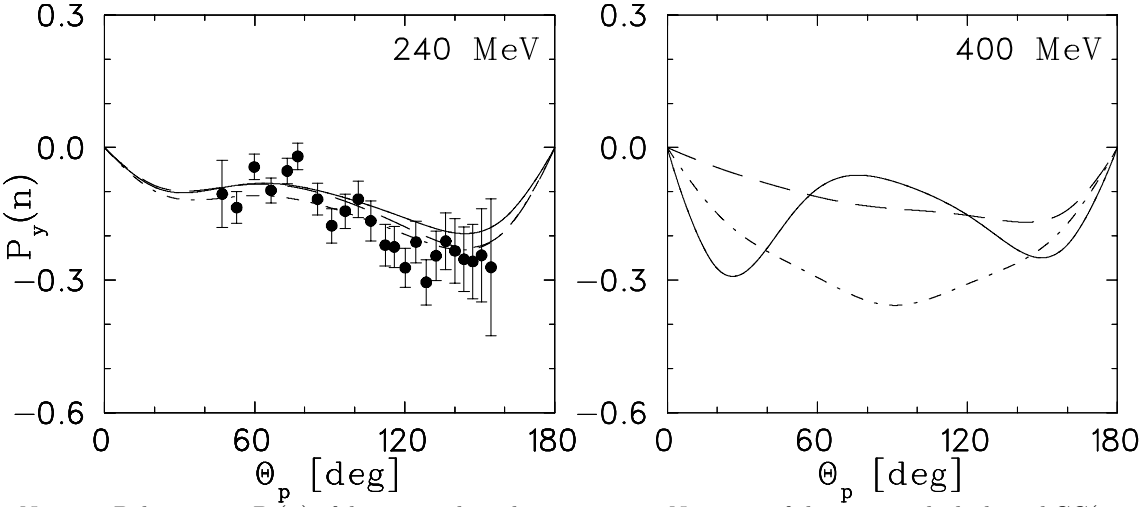

FIG. 25. Neutron Polarization $P_y(n)$ of deuteron photodisintegration. Notation of the curves: dash-dotted CC(stat3), dashed CC(ret4), full CC(ret2). Experimental data from [37] (●).

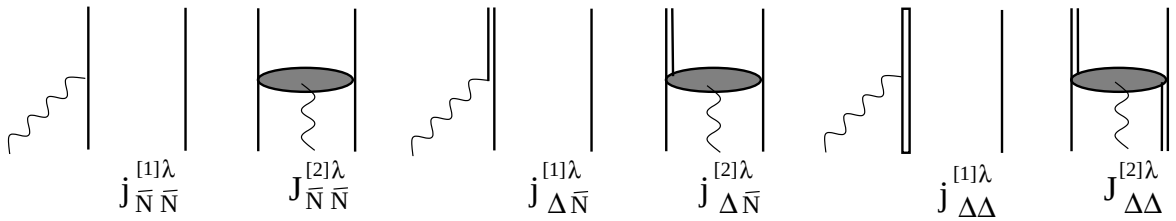
$j^{[1]\lambda}_{\bar{N}\bar{N}}$
$J^{[2]\lambda}_{\bar{N}\bar{N}}$
$j^{[1]\lambda}_{\Delta\bar{N}}$
$j^{[2]\lambda}_{\Delta\bar{N}}$
$j^{[1]\lambda}_{\Delta\Delta}$
$J^{[2]\lambda}_{\Delta\Delta}$

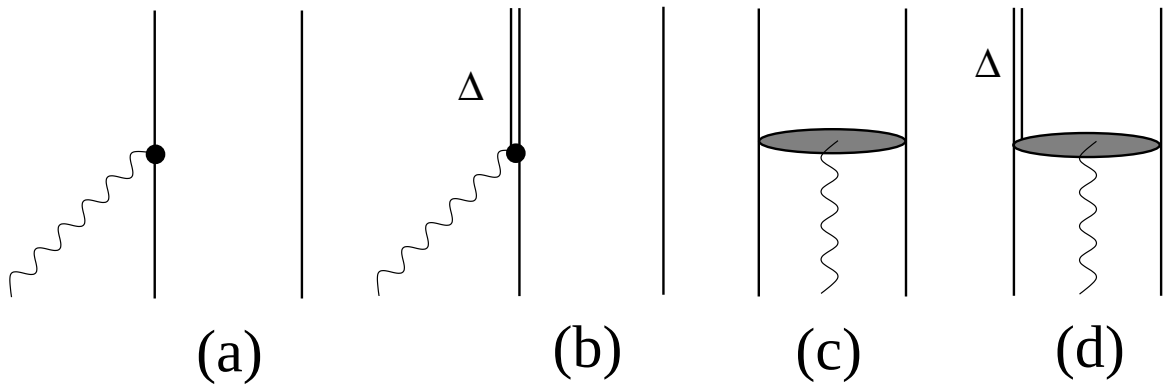
Δ
Δ
(a)
(b)
(c)
(d)

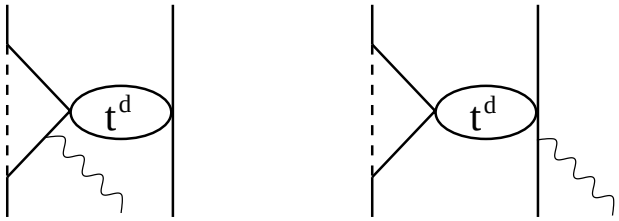
t^d
t^d

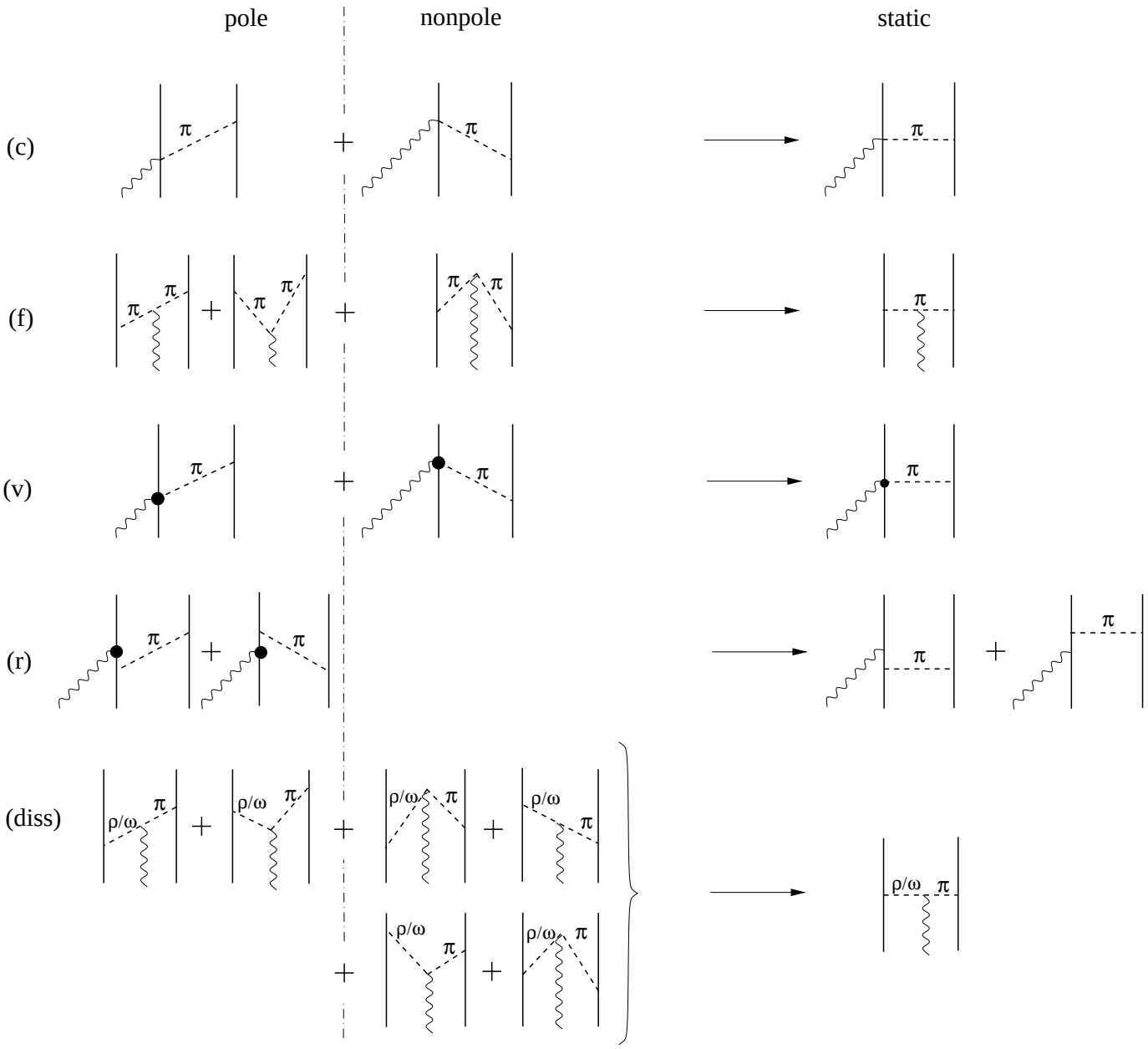
pole
nonpole
static
(c)
(f)
(v)
(r)
(diss)
π
ρ/ω

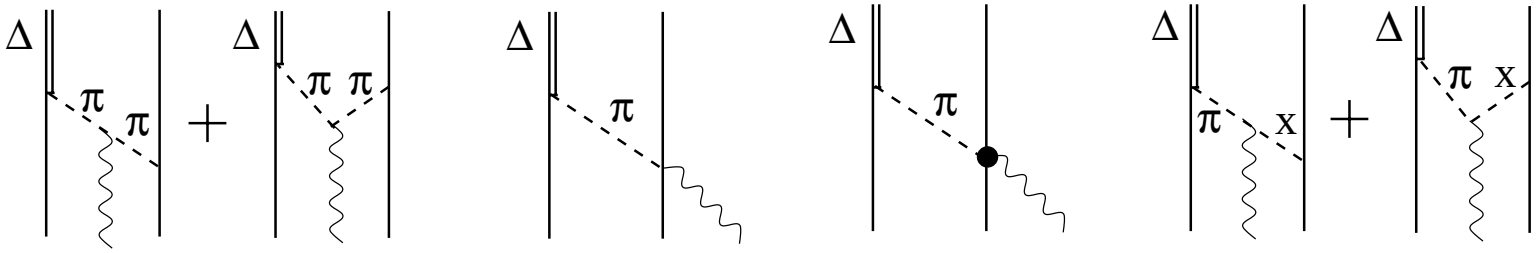
Δ
π
π
+
Δ
π
π
(a)
Δ
π
(b)
Δ
π
(c)
Δ
π
x
+
Δ
π
x
(d)

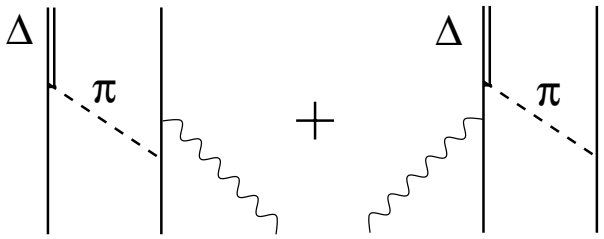
Δ
π
+
Δ
π

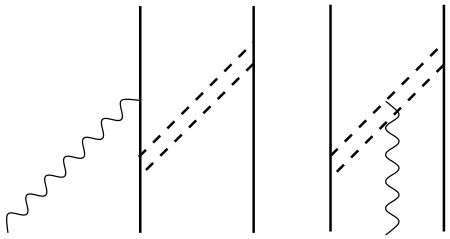

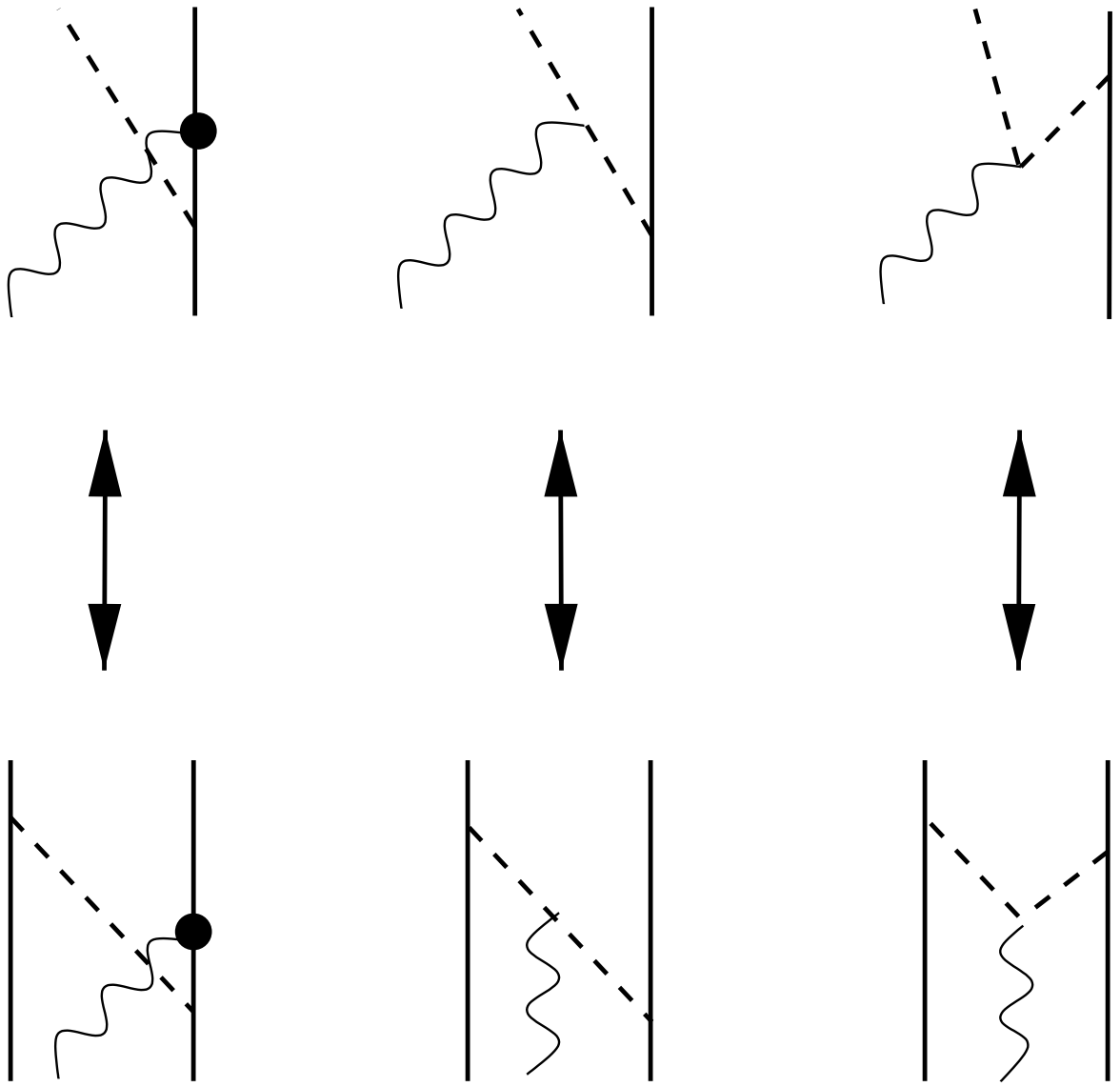

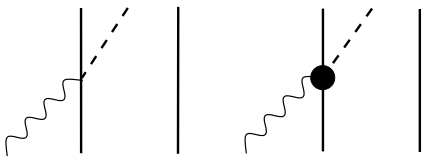

(a) (b)

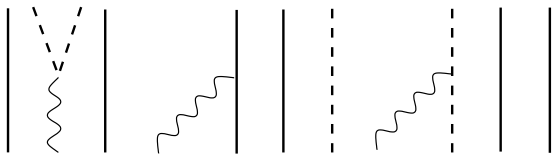
(a)
(b)
(c)

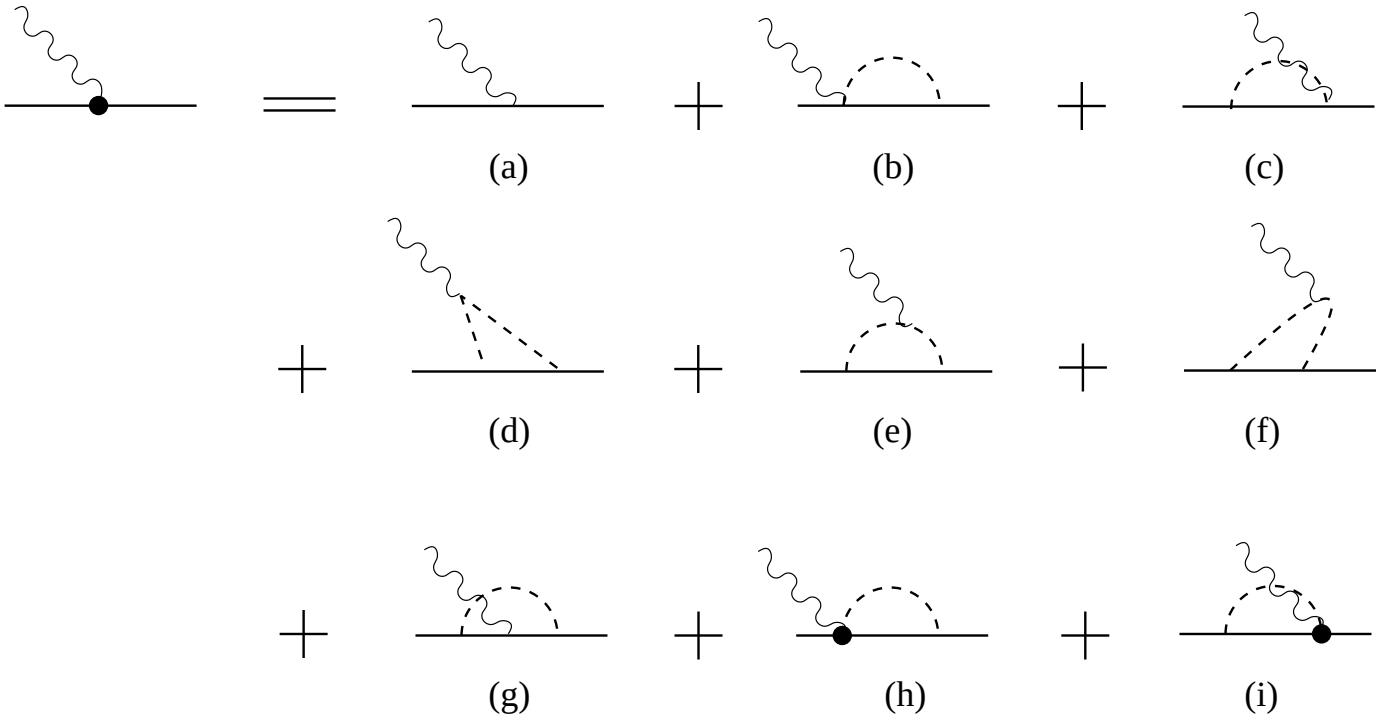
(a)
(b)
(c)
(d)
(e)
(f)
(g)
(h)
(i)

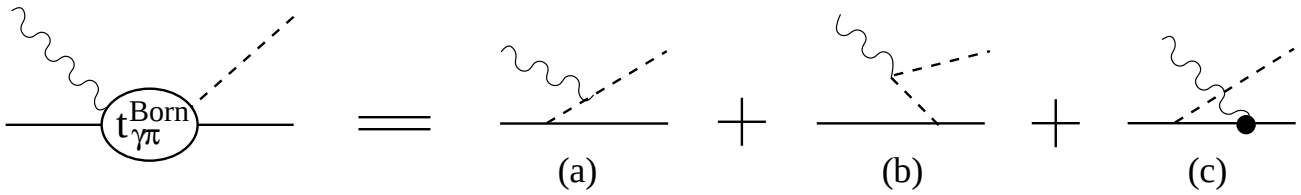
t
Born
γπ
(a)
(b)
(c)

(a)

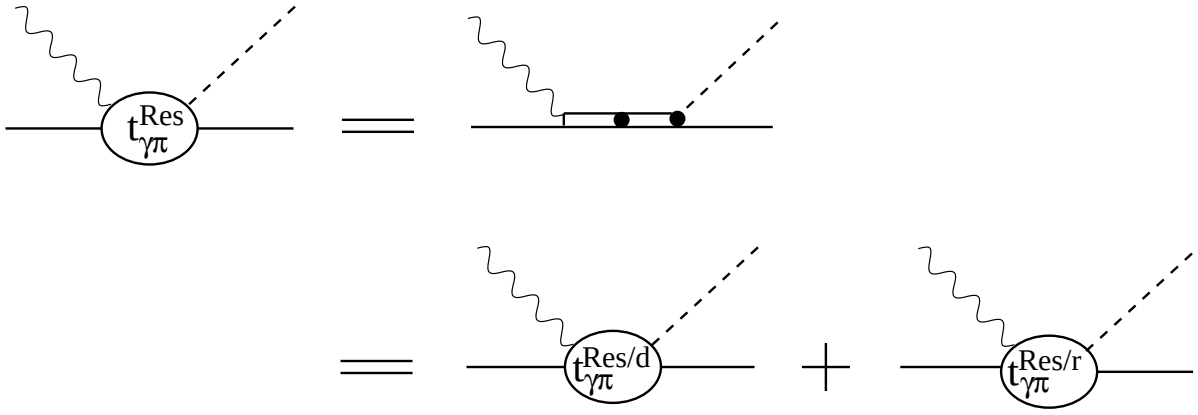
$t^{Res}_{\gamma\pi}$
$t^{Res/d}_{\gamma\pi}$
$t^{Res/r}_{\gamma\pi}$

(b)

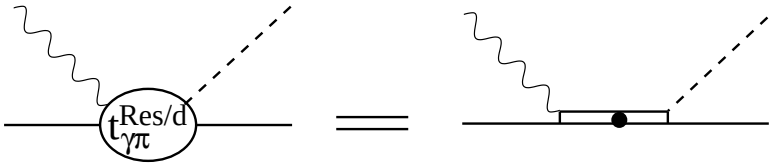
$t^{Res/d}_{\gamma\pi}$

(c)

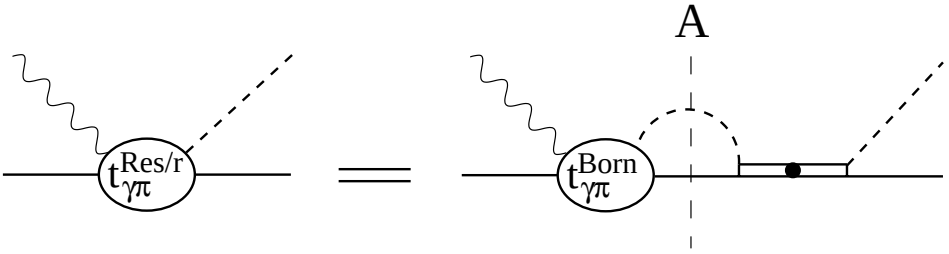
A
$t^{Res/r}_{\gamma\pi}$
$t^{Born}_{\gamma\pi}$